

**REAL TIME PERFUSION AND OXYGENATION MONITORING IN  
AN IMPLANTABLE OPTICAL SENSOR**

A Thesis

by

**HARIHARAN SUBRAMANIAN**

Submitted to the Office of Graduate Studies of  
Texas A&M University  
in partial fulfillment of the requirements for the degree of

**MASTER OF SCIENCE**

December 2004

Major Subject: Biomedical Engineering

**REAL TIME PERFUSION AND OXYGENATION MONITORING  
IN AN IMPLANTABLE OPTICAL SENSOR**

A Thesis

by

HARIHARAN SUBRAMANIAN

Submitted to Texas A&M University  
in partial fulfillment of the requirements  
for the degree of

MASTER OF SCIENCE

Approved as to style and content by:

---

Gerard Coté  
(Chair of Committee)

---

Lihong Wang  
(Member)

---

Henry Taylor  
(Member)

---

William Hyman  
(Head of Department)

December 2004

Major Subject: Biomedical Engineering

## ABSTRACT

Real Time Perfusion and Oxygenation Monitoring in an Implantable Optical Sensor.

(December 2004)

Hariharan Subramanian, B.E., University of Madras

Chair of Advisory Committee: Dr. Gerard Coté

Simultaneous blood perfusion and oxygenation monitoring is crucial for patients undergoing a transplant procedure. This becomes of great importance during the surgical recovery period of a transplant procedure when uncorrected loss of perfusion or reduction in oxygen saturation can result in patient death. Pulse oximeters are standard monitoring devices which are used to obtain the perfusion level and oxygen saturation using the optical absorption properties of hemoglobin. However, in cases of varying perfusion due to hemorrhage, blood clot or acute blockage, the oxygenation results obtained from traditional pulse oximeters are erroneous due to a sudden drop in signal strength. The long term goal of the project is to devise an implantable optical sensor which is able to perform better than the traditional pulse oximeters with changing perfusion and function as a local warning for sudden blood perfusion and oxygenation loss.

In this work, an optical sensor based on a pulse oximeter with an additional source at 810nm wavelength has been developed for *in situ* monitoring of transplant organs. An algorithm has been designed to separate perfusion and oxygenation signals from the composite signal obtained from the three source pulse oximetry-based sensor. The algorithm uses 810nm reference signals and an adaptive filtering routine to separate

the two signals which occur at the same frequency. The algorithm is initially applied to model data and its effectiveness is further tested using *in vitro* and *in vivo* data sets to quantify its ability to separate the signals of interest. The entire process is done in real time in conjunction with the autocorrelation-based time domain technique. This time domain technique uses digital filtering and autocorrelation to extract peak height information and generate an amplitude measurement and has shown to perform better than the traditional fast Fourier transform (FFT) for semi-periodic signals, such as those derived from heart monitoring. In particular, in this paper it is shown that the two approaches produce comparable results for periodic *in vitro* perfusion signals. However, when used on semi periodic, simulated, perfusion signals and *in vivo* data generated from an optical perfusion sensor the autocorrelation approach clearly (Standard Error, SE = 0.03) outperforms the FFT-based analysis (Standard Error, SE = 0.62).

## **DEDICATION**

I would like to dedicate this thesis to my wife, Vidhya, for her guidance, support, love and encouragement. She kept my spirits up when the muses failed me. Without her lifting me up when this thesis seemed impossible, I doubt it should ever have been completed.

## ACKNOWLEDGMENTS

I would like to express my sincere gratitude to my adviser, Dr. Gerard Cote' for financial support and encouragement throughout this research. I would also like to thank my committee members, Dr. Wang and Dr. Taylor, for their guidance during this research. I also wish to thank Bennett Ibey, a Ph.D. student in the Optical Biosensing Laboratory for his useful suggestions and help with Monte Carlo simulations. I also thank all the students of Optical Biosensing Laboratory for their help and support. I would also like to thank Dr. Nance Ericson and his team at Oakridge National lab for their hardware support, Dr. Mark Wilson at the University of Pittsburgh for his clinical support and the Department of Energy for its financial support without which this project would not have been possible.

My parents have constantly encouraged me and guided me to independence, never trying to limit my aspirations. I am grateful to them for their belief in me and their support beyond measure. Finally, I must convey my heartfelt thanks to my wife for her help in every stage of this research work and for being so patient with me.

## TABLE OF CONTENTS

	Page
ABSTRACT .....	iii
DEDICATION .....	v
ACKNOWLEDGMENTS.....	vi
TABLE OF CONTENTS .....	vii
LIST OF FIGURES.....	ix
LIST OF TABLES .....	xii
 CHAPTER	
I    INTRODUCTION.....	1
1.1 Real time analysis of blood perfusion and oxygenation .....	2
1.2 Separation of blood perfusion and oxygenation.....	3
II   BACKGROUND.....	5
2.1 Basic physiology .....	5
2.2 Current measurement techniques .....	7
2.3 Pulse oximeters .....	9
2.3.1 History of pulse oximeters .....	9
2.3.2 Principles of pulse oximetry.....	11
2.3.3 Clinical applications of pulse oximeters .....	16
2.3.4 Limitations of pulse oximeters.....	17
2.4 Autocorrelation based signal processing algorithm .....	18
2.5 Separation of physiologic signals using adaptive filtering....	20
III  THEORY.....	22
3.1 Autocorrelation based time domain technique.....	22
3.2 Extraction of a signal using adaptive filtering.....	25
3.3 Multilayer Monte Carlo modeling of photon transport.....	28

CHAPTER	Page
IV MATERIALS AND METHODS .....	32
4.1 Sensor system design .....	32
4.2 Real time analysis of blood perfusion and oxygenation .....	35
4.2.1 Data simulation .....	35
4.2.2 <i>In vitro</i> system .....	35
4.2.3 <i>In vivo</i> system .....	36
4.2.4 Signal processing .....	38
4.3 Separation of blood perfusion and oxygenation .....	40
4.3.1 Data simulation .....	40
4.3.2 Data collection .....	42
4.3.3 Signal processing .....	43
V RESULTS AND DISCUSSION .....	44
5.1 Real time analysis of blood perfusion and oxygenation .....	44
5.1.1 Data simulation .....	44
5.1.2 <i>In vitro</i> study .....	46
5.1.3 <i>In vivo</i> study .....	50
5.2 Separation of blood perfusion and oxygenation .....	55
VI CONCLUSIONS AND FUTURE WORK .....	69
REFERENCES .....	71
APPENDIX A .....	76
APPENDIX B .....	77
APPENDIX C .....	79
APPENDIX D .....	82
APPENDIX E .....	87
VITA .....	90



## LIST OF FIGURES

FIGURE	Page
1. Extinction coefficients of oxy and deoxy hemoglobin.....	12
2. Mode of operation of pulse oximetry .....	14
3. Red and infrared AC signals at different arterial oxygen saturation .....	15
4. Theoretical calibration curve of pulse oximeter.....	16
5. Block diagram of adaptive filter.....	27
6. Probe containing 3 different LEDs and a photodetector .....	33
7. Block diagram of sensor drive and processing electronics .....	34
8. Custom electronics for sensor interfacing and data collection.....	34
9. Setup for <i>in vivo</i> experiment .....	37
10. Sketch of autocorrelation based perfusion analysis algorithm.....	39
11a. FFT results for simulated data in which perfusion signals mimic the <i>in vivo</i> data.....	45
11b. APAA results for simulated data in which perfusion signals mimic the <i>in vivo</i> data .....	45
12. Raw data from the <i>in vitro</i> system containing the 4Hz signal plus noise from the peristaltic pump .....	46
13. Autocorrelation signal of the raw <i>in vitro</i> data .....	47
14. FFT spectrum of the raw <i>in vitro</i> data.....	47
15. Oxygen saturation from Radiometer .....	48
16a. FFT results for <i>in vitro</i> data showing constant means across 8sec and 4sec split with same blood oxygenation states .....	49
16b. APAA results for <i>in vitro</i> data showing constant mean across 8sec and 4sec split with same blood oxygenation states .....	49

FIGURE	Page
17a. FFT results for <i>in vivo</i> data (660nm source) showing inconsistent means across 8sec and 4sec split with same blood perfusion states .....	50
17b. APAA results for <i>in vivo</i> data (660nm source) showing constant means across 8sec and 4sec split with same blood perfusion states .....	51
18a. FFT results for <i>in vivo</i> data (810nm source) showing inconsistent means across 8sec and 4sec split with same blood perfusion states .....	51
18b. APAA results for <i>in vivo</i> data (810nm source) showing constant means across 8sec and 4sec split with same blood perfusion states .....	52
19a. FFT results for <i>in vivo</i> data (940nm source) showing inconsistent means across 8sec and 4sec split with same blood perfusion states .....	52
19b. APAA results for <i>in vivo</i> data (940nm source) showing constant means across 8sec and 4sec split with same blood perfusion states .....	53
20. An example of the FFT spectrum obtained.....	54
21. Combined oxygenation and perfusion signal using Monte Carlo simulation.....	56
22. Output signals from adaptive filter algorithm .....	57
23. Perfusion signal extracted from first Monte Carlo model data .....	59
24. Oxygenation signal extracted from first Monte Carlo model data.....	59
25. Perfusion signal extracted from first <i>in vitro</i> experiment showing constant perfusion signal while the oxygenation is varying .....	60
26. Oxygenation signal extracted from first <i>in vitro</i> experiment showing varying oxygenation signal while the perfusion is constant .....	61
27. Oxygenation ratio obtained from first <i>in vitro</i> experiment showing increasing oxygenation ratio with decreasing oxygen saturation.....	61
28. Perfusion signal extracted from second <i>in vitro</i> experiment showing increasing perfusion while the oxygenation is constant.....	63

FIGURE	Page
29. Oxygenation signal extracted from second <i>in vitro</i> experiment showing increasing oxygenation with constant ratio .....	63
30. Oxygenation ratio obtained from second <i>in vitro</i> experiment showing constant oxygenation ratio while the perfusion is varying.....	64
31. Perfusion signal extracted from <i>in vivo</i> experiment showing decreasing perfusion state during clamp stage and increasing perfusion in reperfusion stage .....	65
32. Oxygenation signal extracted from <i>in vivo</i> experiment showing decreasing oxygenation with a constant ratio between 660nm and 940nm source .....	65
33. Oxygenation ratio obtained from <i>in vivo</i> experiment showing constant oxygenation ratio with varying perfusion .....	66
34. Plot of oxygen saturation vs ratio in the <i>in vitro</i> experiment showing increasing oxygenation ratio with decreasing oxygen saturation.....	67
35. Plot of oxygen saturation vs ratio in the <i>in vivo</i> experiment showing more stable oxygenation ratio from adaptive filtering.....	67
36. Oxygenation ratio from different analysis techniques showing stable oxygenation ratio compared to traditional analysis techniques .....	68

**LIST OF TABLES**

TABLE		Page
1.	Summary of the range of optical properties used for the model .....	41
2.	Summary of standard error calculated against un-split data .....	54
3.	Summary of the standard error of different analysis techniques.....	68

# CHAPTER I

## INTRODUCTION

In 2002, over 24,000 patients received transplanted organs such as liver, kidney, and intestines [1]. The Scientific Registry of Transplanted Recipients reported first year survival rates for single organ transplants that ranged from 77% for lung transplants to 96% for pancreas transplants. The rate of graft survival was also reported and showed to be on average 10% less than that of the patient survival after the first year [1]. The main reason for patient death is organ malfunction due to complications such as immune rejection [2]. However, one parameter of interest in the transplant procedure is a measure of local blood perfusion and oxygenation within the graft in the days following the transplant. This is because, prolonged and untreated loss of blood perfusion due to acute rejection or mechanical failure (sutures) will result in loss of organ function and be hazardous to the transplant patient [3]. The week following transplant proves the most critical because of high immune response and healing within the organ. Being able to measure the local blood perfusion within a transplanted organ continuously within this crucial period will allow physicians to diagnose organ failure earlier and potentially increase patient and graft survival after surgery [3]. Increasing graft survival will help to prevent multiple transplants (additional organs) and reduce the loss of donated organs and additional surgery. This is important because the number of people on the national waiting list for all organs is significantly higher (>84,000) than the number of available

organs (~24,000) resulting in a constant demand for donated organs [1].

In order to obtain the local blood perfusion information, an *in vivo* sensor to detect the blood perfusion and oxygenation following organ transplant is being developed by the Optical Biosensing Laboratory at Texas A&M University in collaboration with Oak Ridge National Laboratory and the University of Pittsburgh Medical School [4]. The sensor is based on a modified pulse-oximeter that can be implanted onto the transplant organ during the surgical procedure and remain in the body throughout the recovery period. The signal is proposed to be sent from the sensor to a desktop computer or medical readout device by a miniature telemetry system for further processing in order to obtain physiological information [3].

### **1.1 Real time analysis of blood perfusion and oxygenation**

The primary goal of the thesis is the design of a new time domain analysis package based on autocorrelation that is employed to obtain the perfusion and oxygenation signals in real time. Various signal processing techniques including the Fast Fourier transform (FFT), discrete cosine transform, and discrete wavelet have been used to process the pulse oximetry data [5], [6]. FFT and Discrete wavelet transforms average the signal obtained in the form of sinusoids and wavelets, respectively. These signal-processing techniques have some limitations, notably small changes in blood perfusion over a small period of time (less than temporal resolution) cannot be observed. Hence a time-domain technique that is able to resolve small perfusion changes in real time would be ideal and enable better perfusion monitoring leading to improved post-operative care. A second and more noticeable drawback of the FFT based signal processing methods is

the tradeoff between frequency and time resolution [5]. Of specific interest is the inability of the FFT to discriminate between two frequencies that are very close together, as is commonly observed in the natural variability of the heart rate [6]. These frequency fluctuations cannot be resolved accurately meaning that the perfusion or oxygenation signal measured at a random frequency will be averaged resulting in inconsistent perfusion or oxygenation measurements for equal flow states of slightly differing pulse rates. These drawbacks have led us to investigate signal-processing techniques in the time domain rather than in the frequency domain, specifically autocorrelation. The time domain analysis package is designed to capture the semi-periodic blood flow signal in the presence of large background noise.

This signal processing package uses digital filtering and autocorrelation to extract peak height information and generate an amplitude measurement. The autocorrelation based time domain technique (S.E=0.03) has shown to perform better than the FFT (S.E=0.62) for semi-periodic signals, such as those derived from heart monitoring. In particular, in this work it is shown that the two approaches produce comparable results for periodic *in vitro* perfusion signals. However, when used on semi periodic, simulated, perfusion signals and *in vivo* data generated from an optical perfusion sensor the autocorrelation (S.E=0.006) approach clearly outperforms the FFT-based analysis (S.E=0.128) [7].

## **1.2 Separation of blood perfusion and oxygenation**

Traditionally pulse oximeters isolate an oxygenation value using a simple ratio between the two wavelengths of light assuming constant perfusion. However, in cases of

varying perfusion due to hemorrhage, blood clot or acute blockage, oxygenation results obtained from commercial pulse oximeters are erroneous due to sudden drop in signal strength. This becomes of great importance during the surgical recovery period of a transplant procedure when uncorrected loss of perfusion can result in patient death.

The second goal of the thesis will be on the separation of the oxygenation signal from the composite pulse oximetry signal that required changes in the traditional hardware and introduction of a new signal processing algorithm based on adaptive filtering. In order to account for unpredictable perfusion changes, an additional source at 810nm is used. At this wavelength, it is assumed that the total absorbance of the sample does not change due to oxygen saturation but only due to blood perfusion. The newly developed algorithm was tested using Monte Carlo simulated data to prove the effectiveness of the 810nm reference. Following these tests, an *in vitro* model was generated that isolated the effects of perfusion and oxygenation allowing testing of the sensor on real tissues and whole blood. The sensor accurately captured changes in oxygenation and perfusion using this setup with reliable consistency. Using the serosal surface of the swine jejunum, *in vivo* data was taken to analyze the sensors response to fluctuating perfusion levels like that seen in hemorrhaging or failing transplants. Overall, it was shown that the addition of an adaptive filtering algorithm (S.E=0.06) to the existing processing package has improved the sensors stability and improved its overall accuracy than when used without any filtering (S.E=0.20) [8].



## **CHAPTER II**

### **BACKGROUND**

The first section of this chapter covers the basic physiology of blood oxygen transport followed by a section on the measurement techniques which are currently being used to monitor blood perfusion and oxygenation. The third section details the history of pulse oximeters, the principle, application and the limitations of pulse oximetry technique. The final section gives an overview of the autocorrelation based time domain approach and the separation of physiologic signals using adaptive filtering that is used in this research.

#### **2.1 Basic physiology**

Oxygen is essential for the proper functioning of each cell in the human body. The absence of oxygen for a prolonged period of time (hypoxia) will result in cell death and hence loss of organ or tissue functions [9]. Oxygen is delivered to different parts of the body by the blood stream with the help of red blood cells. Transport of oxygen is affected by different factors such as the availability of oxygen to the lungs, the ability of oxygen to pass the alveolar/capillary membrane, and the capacity of the blood to carry oxygen. Once oxygen is supplied to various parts of the body by the blood stream, the deoxygenated blood is brought back to the lungs through arterial capillaries where exchange of gases takes place. The blood rids itself of carbon-dioxide and receives oxygen in the lungs. The process of respiration provides a continuous supply of oxygen

to the lungs. The reoxygenated blood is then recirculated throughout the body with the help of circulatory system [9].

The most important feature that enables the blood to transport oxygen is the hemoglobin found within the red blood cells. A hemoglobin molecule consists of two parts namely the globin portion and a heme group. The globin portion is a protein made up of four highly folded polypeptide chains. The heme group is a non protein group containing four iron molecules, which in turn is bound to one of the polypeptides. Each of the four iron molecules combine irreversibly with an oxygen molecule. Thus each hemoglobin molecule carries four oxygen molecules from the lungs to different parts of the body. Because of the presence of iron molecule, hemoglobin appears reddish in color when combined with oxygen and appears bluish when deoxygenated. Hence a fully oxygenated arterial blood is red in color while the deoxygenated venous blood is bluish [10]. Thus deoxygenated blood absorbs more red light than the oxygenated blood. Pulse oximeters takes advantage of this physiologic information to non-invasively detect the oxygen content in blood.

Oxygen is carried in two ways throughout the body. It can be dissolved in the plasma of the blood and transported by the blood stream. This method constitutes a very small part of the oxygen supplied (~10%) to the cells but it does give the clinician an idea about the amount of oxygen passing through the alveolar/capillary membrane. The partial pressure of oxygen ( $pO_2$ ) measures the dissolved portion of oxygen in the blood. Another method of oxygen transport, oxygen saturation ( $SO_2$ ), is where oxygen binds to the hemoglobin molecule within the red blood cells [11]. The majority of oxygen is

carried by the hemoglobin molecules. Hence the measures of amount of blood supplied to the tissue by the capillaries (blood perfusion) as well as the oxygen carried in the blood (oxygen saturation) are two important indicators of a patient's health. The primary goal of this project is to design an optical sensor that can simultaneously monitor the blood perfusion as well as the blood oxygen saturation in transplant organs.

## **2.2 Current measurement techniques**

Different chemical and optical methods have been used to determine the oxygen content of the blood. Some of the chemical methods like the Van Slyke method, Mixing syringe method, Clark electrode and galvanic electrode find the partial pressure of oxygen ( $pO_2$ ) to determine the oxygen content of the blood [12], [13]. Spectrophotometers and CO-oximeters are some of the optical methods that are used to measure the oxygen saturation of the blood ( $SO_2$ ) [14]. Oximetry is a general term that refers to the optical measurement of oxyhemoglobin saturation of the blood. Spectrophotometry is the basis for all oximetry techniques [9]. It works on the principle that atoms of all molecules vibrate in a specific pattern that is unique for each substance. As the light is passed through a substance, the frequency of light similar to the vibration frequency of the substance is absorbed while all the other frequencies are transmitted or reflected. Spectrophotometers measure the intensity of light transmitted through a substance at a particular wavelength. Since oxyhemoglobin ( $HbO_2$ ) and deoxy-hemoglobin ( $Hb$ ) absorb light at certain wavelengths, the oxygen saturation can be obtained from the ratio between these hemoglobin species (expressed in percentage) [9].

The ability to detect capillary blood flow, known as blood perfusion, has many potential clinical applications. Blood perfusion is primarily used to detect sites of tumors and rejected transplanted organs [15]. Several modalities like radioactive tracers, ultrasound Doppler, laser Doppler and plethysmography techniques are primarily used to detect blood perfusion. Regional perfusion can also be monitored using serum creatinin levels and serum bilirubin levels in the blood [9]. Laser Doppler flowmeter (LDF) and Photo-plethysmography are the popular optical techniques of measuring blood perfusion in tissues. LDF is a non-invasive technique capable of continuously measuring blood circulation. Laser light propagated into a tissue containing flowing blood is scattered differently causing a Doppler shift that is detected and representative of blood velocity. The main drawback of this technique is that it does not provide any information about oxygen saturation of the blood and cannot diagnose the health of the blood [16]. LDF has also shown success in measuring microvascular perfusion but remains too cumbersome to be used *in vivo* [6].

Photoplethysmography (PPG) provides a qualitative measure of the tissue blood volume increase or decrease. It works on the principle of pulse oximetry by measuring the light transmission through the tissue as a function of time during systole. PPG oscillates with the heart cycle period, due to the systolic increase in the tissue blood volume, resulting in a lower transmission of light [17]. Thus by measuring the amount of light reflected or transmitted back to the detector, the relative amount of blood present in the blood vessels can be obtained. The main drawback of this method is that it gives only

a relative measurement of the blood volumetric changes but not the exact amount of blood [17].

The sensor system involved in this project, to measure blood perfusion and oxygenation, is designed based on the principle of pulse oximetry. The following section describes the principles of pulse oximetry, the clinical applications and its limitations.

### **2.3 Pulse oximeters**

Pulse oximeters have been commercially available for more than 20 years and have become a standard monitoring device in hospital critical care units and surgical suites [9]. Unknown in the operating room before the 1980s, the pulse oximeters, whose operation requires no special training or new skills on the part of the user, has rapidly become a minimum standard of anesthetic care [18].

#### *2.3.1 History of pulse oximeters*

The history of pulse oximeters dates back to the 1930s when Matthes built the first device that can continuously measure blood oxygen saturation *in vivo* by transilluminating the tissue. Two wavelengths of light at visible and infrared were used to track the changes in oxygenation similar to the modern day pulse oximeters. The first wavelength was sensitive to changes in oxygenation while the second wavelength at infrared was less sensitive and thus was primarily used to compensate for changes in tissue thickness, hemoglobin content and light intensity [18]. This instrument could follow the saturation trends but was difficult to calibrate. Squires *et al.* developed a similar instrument that can calibrate itself by compressing the tissue to remove blood

[19]. A similar calibration technique was later adopted in the first commercially marketed *in vivo* oximeters [18].

The term ‘oximeter’ was first coined by Glen Millikan to describe a light weight device that he developed for aviation research [18]. In the 1940s Wood *et al.* developed a similar instrument that was used in the operating rooms to detect significant desaturations during routine anesthetics [20]. A paper published in *Anesthesiology* (1951) concluded that “on many occasions this instrument has detected anoxemia when observation of pulse, blood pressure, and color of the patients, and peripheral vascular tone have shown no abnormalities” [21]. The early *in vivo* oximeters were not widely accepted by clinicians because of their severe limitations. These were delicate instruments that required a technician for its operation and maintenance. Furthermore, it required calibration on each patient prior to its use.

In the 1970s Hewlett-Packard marketed their first self calibrating ear oximeters. The device used eight wavelengths of light to determine the hemoglobin saturation [22] and soon became a standard clinical and laboratory tool in pulmonary medicine. The size, cumbersome nature of the ear probes and the expense of the oximeters prevented its acceptance in operating rooms.

The first pulse oximeter was invented by Takuo Aoyagi in the mid 1970’s. He was developing a method of semi-noninvasively estimating the cardiac output by detecting the washout curve of dye injected into a peripheral vein as it perfused the ear. He noticed pulsation in the washout curves due to the arterial pulse in the ear. When subtracting these pulsations from the washout curve he discovered that the absorbance

ratio of the pulsation at the two wavelengths of red and infrared changed with arterial hemoglobin saturation. The discovery soon led him to the creation of the first two wavelength pulse oximeters based on pulsatile light absorbances [18]. Aoyagi's oximeters used filtered light sources and fiberoptic cables to transmit light between the instrument and ear sensor. This cumbersome design made it difficult to use in operating rooms. In the late 1970s Scott Wilbur of the Biox corporation designed an ear sensor that used light emitting diode and solid state photodetectors to develop a clinically accepted pulse oximeter. The fiberoptic cables of previous ear oximeters were replaced by a thin electrical cable. The accuracy of the pulse oximeters was also improved by incorporating digital microprocessors into the instrument. Further improvements in reliability and inexpensive cost made pulse oximeters a standard operating room monitor [18].

Modern day pulse oximeter uses two different light sources at red and infrared wavelength to obtain oxygen saturation information. These pulse oximeters use finger as the main probing area rather than the ear as was used in the previous pulse oximeter models. The light is supplied to the probing area using an electric probe and the data is processed in real time using online microprocessor present in the instrument. This makes the pulse oximeters popularly used in emergency care of patients as the physicians can obtain heart rate and blood oxygenation information simultaneously in real time.

### *2.3.2 Principles of pulse oximetry*

Pulse oximeters are based on two important physical principles: 1) The presence of a pulsatile signal generated by the arterial blood, which is relatively independent of

non-pulsatile arterial blood, venous and capillary blood, and other tissues and 2) Oxyhemoglobin (HbO<sub>2</sub>) and reduced hemoglobin (Hb) have different absorption spectra. Traditional oximeters use two light emitting diodes that emit light at 660nm (red) and 940nm (infrared) wavelengths. At these wavelengths both oxyhemoglobin and reduced hemoglobin have different absorption spectra (Fig. 1). The ratio of absorbances at these two wavelengths are then used to estimate arterial blood oxygen saturation (Eqn. 1). The curves obtained from the absorbances are calibrated empirically against direct measurements of blood oxygen saturation in volunteers to arrive at a calibration algorithm that is then used to generate pulse oximeter's estimate of arterial saturation.

$$\text{Ratio, } R = \frac{\text{Absorbance}_{red}}{\text{Absorbance}_{IR}} \quad (1)$$

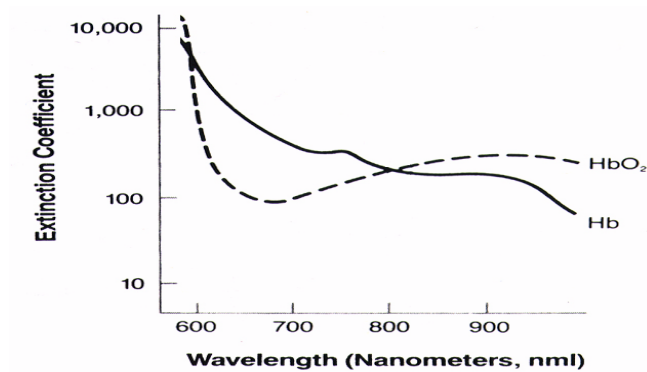


**Fig. 1.** Extinction coefficients of oxy and deoxy hemoglobin [23]

The operations of oximeters in general are based on the Beer-Lambert law, which relates the concentration of the solute to the intensity of light transmitted through a solution.

$$I_{out} = I_{in} \exp [-(\epsilon CL)] \quad (2)$$



where  $I_{\text{out}}$  and  $I_{\text{in}}$  are the intensities of transmitted light and incident light respectively.

$\epsilon$  is the extinction coefficient or absorptivity of the solute (a constant for a given solute at a specified wavelength),  $C$  is the concentration of the solute (hemoglobin) and  $L$  is the distance the light is transmitted through the liquid (path length). The extinction coefficient  $\epsilon$  is a property of light absorption for a specific substance at a specified wavelength. The extinction coefficient can vary dramatically with the wavelength of light. The concentration  $C$  is measured in  $\text{mmol L}^{-1}$  and the extinction coefficient is expressed in  $\text{L mmol}^{-1} \text{cm}^{-1}$  [9]. Beer's law is based on the property that the sum of the transmitted and absorbed light equals the incident light. This does not account for the reflection of the light at the surface of the medium or scattering of light in the medium.

Laboratory *in vitro* oximeters use this principle to measure the concentration of hemoglobin solution filled in a cuvette produced from lysed red blood cells [24] by measuring the intensity of light transmitted. Pulse oximeters estimate the arterial hemoglobin saturation by measuring the transmission of light at two wavelengths through a pulsatile vascular tissue bed. Pulse oximeters use living tissues such as ear or finger as the 'cuvette' containing hemoglobin, but the living tissues contain many light absorbers such as skin, soft tissue, venous and capillary blood other than the arterial hemoglobin to be estimated (Fig. 2). Early oximeters compressed the soft tissues to compensate for the additional tissue absorbance. The absorbance of bloodless tissue was used as a base line to estimate absorption from the arterial blood. Some oximeters also heated the tissue during measurement to render it hyperemic and thus obtaining an absorbance that is more dependent on the arterial blood.

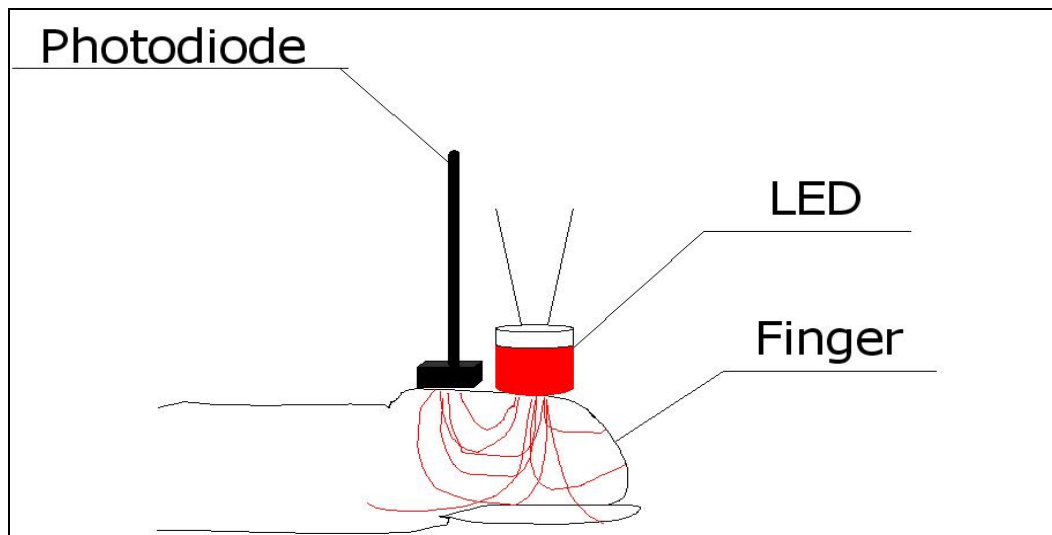


**Fig. 2.** Mode of operation of pulse oximetry

Pulse oximeters distinguish the absorbance of arterial blood and other absorbers in a novel way. The absorbance of arterial blood pulsations are similar to an ‘alternating current’ or simply an AC component while the absorbance from other tissue are always a constant termed as the DC component similar to a ‘DC current’. The AC component pulsations are caused by the systolic volume expansion of the arteriolar bed, which causes the increase in optical path length thus increasing the absorbance. Pulse oximetry is based on the assumption that the arterial blood is the only source of pulsatile absorbance while any other fluctuating light absorbers will act as a source of error. Fig. 3 shows the AC signals of red and IR signals at different oxygen saturation (0%, 85% and 100%). The height of the AC signal varies between the red and IR signals due to the difference in absorption between the oxy and deoxy hemoglobin at red and IR wavelengths.

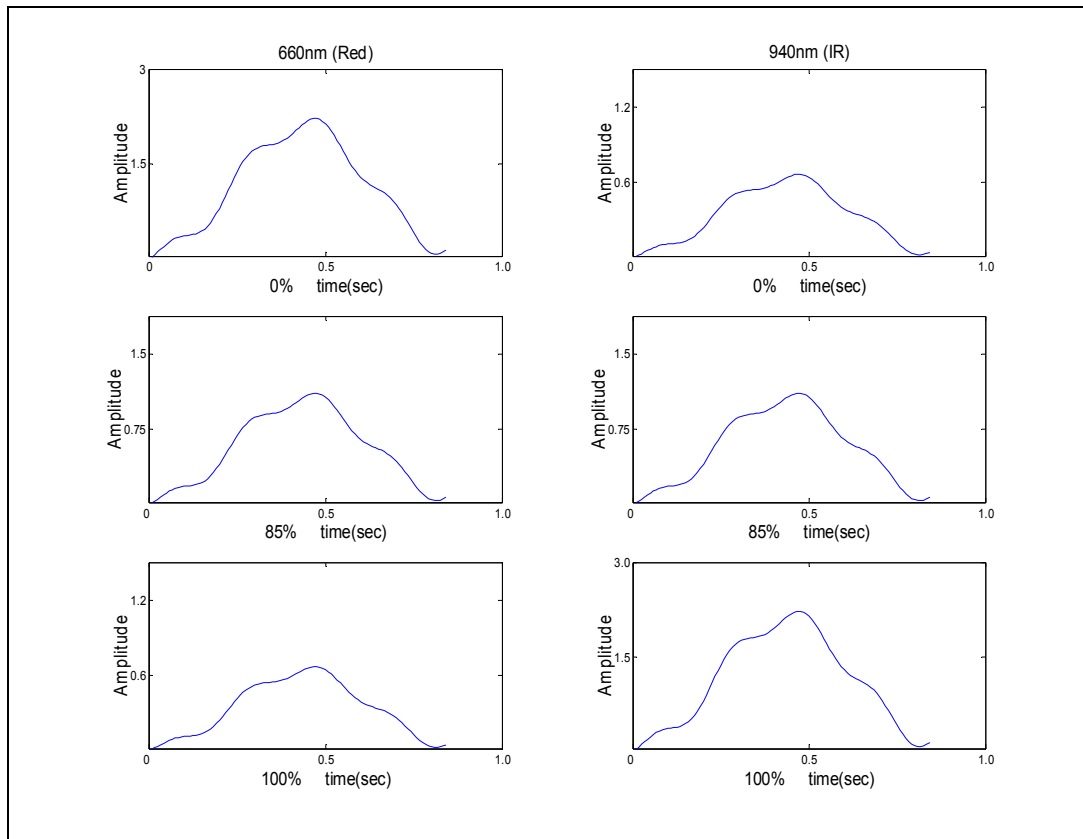


**Fig. 3.** Red and infrared AC signals at different arterial oxygen saturation

The ratio  $R$  in equation 1 can be rewritten as follows,

$$Ratio, R = \frac{AC_{red}/DC_{red}}{AC_{IR}/DC_{IR}} \quad (3)$$

The ratio  $R$  is uniquely related to the arterial hemoglobin saturation. Fig. 4 shows the theoretical calibration curve of the pulse oximeter obtained from Beer's law.

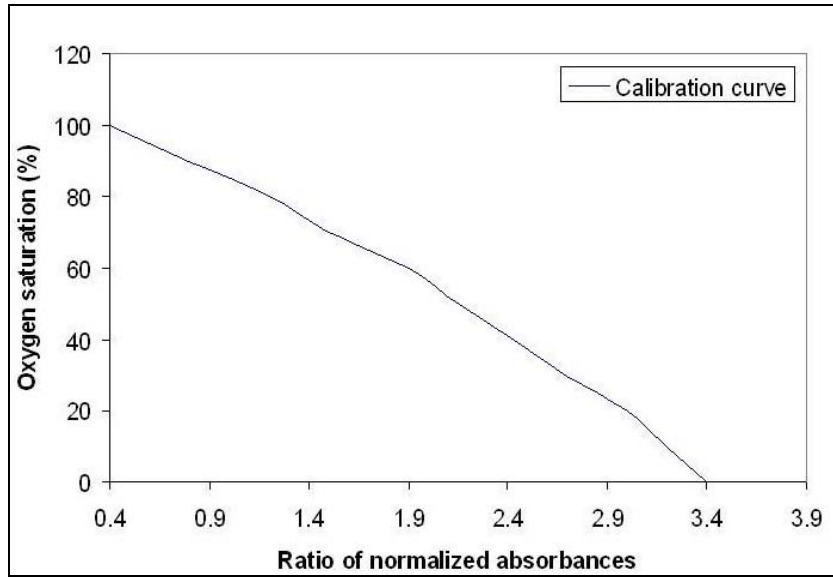


**Fig. 4.** Theoretical calibration curve of pulse oximeter

The pulse oximeter saturation  $SpO_2$  can be empirically derived using the value of  $R$  given the empirical calibration curve relating  $SpO_2$  to  $R$ . The oxygen saturation,  $S$  is written in terms of the ratio  $R$  as follows:

$$S = \frac{a_{r1} - a_{r2}R}{(a_{r1} - a_{o1}) - a_{r2} - a_{o2}R} \quad (4)$$

where  $a_{r1}$ , and  $a_{r2}$  are the molar absorptivity of de-oxy hemoglobin at red and infrared wavelength, while  $a_{o1}$  and  $a_{o2}$  are the molar absorptivity of oxy hemoglobin at red and infrared wavelength.

### 2.3.3 Clinical applications of pulse oximeters

Modern pulse oximetry is a noninvasive, easy to use and accurate procedure to obtain valuable physiological information such as blood oxygen saturation, heart rate, and blood flow information. Pulse oximetry is commonly used when administering

anesthesia, during patient transport, for pediatric care and for veterinary medicine. Some of these applications require special add on equipment and/or special calibration of the pulse oximeter.

As an example during desaturation of the blood its use for anesthesia monitoring, Moller *et al.* observed that during this phase, arterial oxygen saturations decrease to 90% or less with a frequency of 25% in patients [25]. Pulse oximetry can thus detect this desaturation in real time indicating the need for increasing the mixture of oxygen given to the patients during surgery. Use of pulse oximeters has also been reported in many surgical procedures like abdominal, thoracic and dental surgeries to monitor arterial desaturation occurring during surgery [26].

Pulse oximeters have also been used to monitor tissue blood supply and organ viability. MacDonald *et al.* used pulse oximetry to monitor the intestinal blood flow in dogs and tested the intestinal viability after surgery [27]. When transferring tissues such as skin and muscle flaps, it is important to monitor the tissue for adequate supply of blood. Transferred muscle flaps have been monitored via pulse oximetry for 24 to 48 hours to determine the chances of survival [28]. Lastly, specially designed pulse oximeters are being used in ambulances to monitor the vital conditions of patients and during child birth for fetal monitoring [29], [30].

#### *2.3.4 Limitations of pulse oximeters*

Motion artifacts, skin pigmentation and low perfusion states are some sources of error that may lead to inaccurate readings in pulse oximetry [18]. Since pulse oximeters primarily employ two wavelengths they are used to distinguish two substances deoxy

hemoglobin and oxy hemoglobin. The oxygen saturation in blood is also affected by other types of hemoglobin such as carboxyhemoglobin (COHb) and methemoglobin (MetHb). Elevated levels of COHb overestimates the arterial oxygen saturation obtained from the pulse oximetry while elevated MetHb levels may also cause inaccurate oximetry readings. Hence four wavelengths might be required to distinguish different hemoglobin types that in turn will increase the complexity of the instrument [9].

Intravenous dyes such as methylene blue, indocyanine green and indigo carmine can give falsely low pulse oximetry readings. Motion artifacts continues to be a significant source of error and false alarms [31]. The movement of patients gives an incorrect plethysmograph reading that in turn affects the blood oxygenation ratio given by the pulse oximeter. Various methods have been employed to reject motion artifacts but have met with little success [32]. Low perfusion states such as vasoconstriction, hypothermia and low cardiac output also make it difficult for the sensor to distinguish between the background noise and true signal yielding incorrect oxygenation readings.

This thesis addresses some of these limitations of pulse oximetry that is quite critical for the design of the optical sensor for transplant organs. The signal processing package explained in this thesis is designed to measure the oxygen saturation of the blood at low perfusion states providing consistent oxygenation measurements in the presence of motion artifacts.

## **2.4 Autocorrelation based signal processing algorithm**

Due to the inherent frequency resolution limitations associated with standard FFT analysis [6], and limitations in moving averaging due to motion artifact [5], an

autocorrelation-based signal-processing package was developed as described in this thesis to analyze perfusion data. The package is designed to capture semi-periodic blood flow signals in the presence of large background noise.

Autocorrelation is a statistical technique that has been used as a noise-reduction algorithm in many physiological measurements, including LDF and pulse oximetry [33], [34]. Autocorrelation has been used with LDF to discriminate between the capillary and arterio-venular blood flow in skin perfusion measurements as well as to obtain cell perfusion signals from the brain cortex of anesthetized rats to distinguish fractal noise from motion in physiological data [34], [35]. A conventional pulse Doppler device and an autocorrelation-based signal processing technique has also been used for real time two-dimensional imaging of blood flow [36]. Autocorrelation has also been employed to compensate for eye movement in retinal speckle flowmetry studies and in speech processing to study neural activity (time delayed correlation) [37], [38]. A noise resistant algorithm to reconstruct a pulse oximetry derived signal was constructed by Coetzee *et al.* in order to obtain the heart rate and oxygenation information [39]. This was accomplished by generating a synthetic reference signal based on heart rate and using it to construct an idealized pulse signal. Another group showed the use of autocorrelation to measure heart rate from a ring sensor developed to obtain vital signs of the body [33]. In this method, autocorrelation was used to obtain the pulsatile signal from the non-periodic noisy data and its periodicity was then estimated to obtain the heart rate.

## 2.5 Separation of physiologic signals using adaptive filtering

Extraction of a physiologic signal or elimination of noise from a composite signal poses a great challenge for biological signals. If a description of either the signal or noise portion is available, then adaptive noise canceling techniques can be used to remove either the noise or the actual signal portion from composite signal leaving the remaining portion for further analysis [40]. Adaptive filters have been successfully used with biological signals to extract noise from a composite signal [40], [41]. Diab *et al.* developed a signal processing apparatus to generate a primary or secondary reference signal to extract either the primary or secondary signal portion from the composite signal using correlation cancellers such as an adaptive noise canceller. Time sequenced adaptive filters (TSAF) were used by Thaler *et al.* to record the morphology of fetal electrocardiograms (FECG) [42]. TSAF use recordings from the abdomen and chest, to produce a measurement system which rejects the maternal ECG and enhances the FECG. This group reported a relatively noise free FECG waveform with minimal change of parameters. Sison *et al.* used an adaptive filtering technique to characterize motion artifacts in both pulse oximetry and ECG signals. They compared two different adaptive filtering techniques in order to study the effectiveness of the algorithm for noise removal [43], [44]. In most of these cases, the reference signal was obtained from an external source which was then used to extract pure signal using adaptive filters. It was the intention of this group that the addition of the 810nm source would allow for use of an adaptive algorithm in eliminating the need for an external source.



In order to address the limitations of pulse oximetry at very low perfusion states this additional wavelength at 810nm has also been used to separate the oxygenation and perfusion signals. This point in the wavelength spectrum is known as the isosbestic point [45] (Fig. 2). By this change in the traditional hardware of pulse oximetry, the oxygenation signal could be measured under unpredictable perfusion changes. Previous work by our group, Ibey *et al.* [46], has focused on evaluating the effectiveness of adding a third source centered at 810nm into the traditional pulse oximeter. The hypothesis was that by adding a light emitting diode centered near the isosbestic point, a third independent measurement would be made that was relatively oxygen insensitive. This third wavelength would allow for the removal of motion artifact and perfusion signal from the composite signal. It was shown using a Multi-Layer Monte Carlo model (MLMC) and *in vitro* blood flow phantom that a broadband diode centered at 810nm is only slightly affected by changes in blood oxygenation [46].

In pulse oximetry, the use of non-traditional wavelengths has also been explored to evaluate the effect of other molecules in the blood. Hammer *et al.* had reported the use of three isosbestic points (522nm, 569nm and 586nm) to compensate the non-hemoglobin absorption and scattering [47]. The three isosbestic points were used as reference spectra to obtain the oxygen saturation values from *in vivo* spectra measured at the ocular fundus. Buinevicius *et al.* had designed a three wavelength pulse oximeter to determine carboxy-hemoglobin (COHb) concentration. They used an additional LED at 810nm to determine the amount of COHb in blood and a method to calibrate the pulse oximeter for three wavelengths was also presented [48].

## CHAPTER III

### THEORY

The first section this chapter explains the principle of autocorrelation which is used as a real time signal processing package to monitor perfusion and oxygenation signals in this research. The separation of physiological signals using an adaptive noise cancellation technique is explained in the second section. The final section describes the Monte Carlo method of simulating photon transport in biological tissues to model the perfusion and oxygenation signals obtained at the detector end.

#### 3.1 Autocorrelation based time domain technique

The autocorrelation-based signal processing package was developed to analyze the perfusion and oxygenation data in real time. The package captures semi-periodic blood flow signals in the presence of large background noise. Cross correlation is a common signal processing tool used to extract information related to the correlation of two signals. Autocorrelation is a special case of cross correlation where the correlation is performed between the same signals [49]. In general, the autocorrelation method would extract periodic signals buried in random non-periodic noise [33]. In our case it extracts the aperiodic information and assigns the rate of the signal as the size of the window to obtain amplitude information of the pulse oximetry signal.

The cross correlation  $R_{xy}(l)$  of real signal sequences  $x(n)$  and  $y(n)$ , having finite energy, is shown below in Eqn. 5.

$$R_{xy}(l) = \sum_{n=-\infty}^{\infty} x(n)y(n-l), \quad \text{where } l = 0, \pm 1, \pm 2, \dots \quad (5)$$

In the above equation,  $x$  and  $y$  represent the sequences being correlated and the index  $l$  represents the time shift or lag parameter. In the above case the sequence  $x(n)$  is unshifted while the sequence  $y(n)$  is shifted  $l$  units (left for  $l$  positive and right for  $l$  negative). Equivalently,  $x(n)$  may be shifted to right or left by  $l$  units with  $y(n)$  being unshifted.

The autocorrelation is a special case, where  $x(n)$  and  $y(n)$  are the same signal sequence (Eqn. 6).

$$R_{xx}(l) = \sum_{n=-\infty}^{\infty} x(n)x(n-l), \quad \text{where } l = 0, \pm 1, \pm 2, \dots \quad (6)$$

Eqn. 7 and Eqn. 8 represent the cross correlation and autocorrelation for  $x(n)$  and  $y(n)$  as power signals.

$$R_{xy}(l) = \lim_{N \rightarrow \infty} \frac{1}{2N+1} \sum_{n=-N}^N x(n)y(n-l) \quad (7)$$

$$R_{xx}(l) = \lim_{N \rightarrow \infty} \frac{1}{2N+1} \sum_{n=-N}^N x(n)x(n-l) \quad (8)$$

Of specific importance in noise reduction is the fact that the autocorrelation of a repetitive signal with period  $K$  is also repetitive with period  $K$  (Eq. 8.).

$$x(n+K) = x(n) \quad (9)$$

$$R_{xx}(l+K) = \lim_{N \rightarrow \infty} \frac{1}{2N+1} \sum_{n=-N}^N x(n)x(n-l-K) = R_{xx}(l) \quad (10)$$

In some practical applications, correlation is used to identify repetitions in an observed signal that may be corrupted by random interference. For example, let the signal arriving at the detector be represented by  $y(n)$  which can be represented as a

combination of the pulse oximetry signal  $x(n)$  and a non-periodic noise  $w(n)$  (Eqn. 11).

The autocorrelation sequence of  $y(n)$  is shown in Eqn. 12.

$$y(n) = x(n) + w(n) \quad (11)$$

$$R_{yy}(l) = \lim_{N \rightarrow \infty} \frac{1}{2N+1} \sum_{n=-N}^N y(n)y(n-l) \quad (12)$$

If  $y(n)$  is a repetitive sequence with period  $N$ , the averages indicated in the above equation over the long finite interval are identical to the average over a single repetition (Eqn. 7). Substituting  $y(n)$  from Eqn. 5 into Eqn. 13 yields Eqn. 14. This can be simplified into Eqn. 15, which represents the complete autocorrelation of the original signal.

$$R_{yy}(l) = \frac{1}{N} \sum_{n=0}^{N-1} y(n)y(n-l) \quad (13)$$

$$R_{yy}(l) = \frac{1}{N} \sum_{n=0}^{N-1} [x(n) + w(n)][x(n-l) + w(n-l)] \quad (14)$$

$$\begin{aligned} &= \frac{1}{N} \sum_{n=0}^{N-1} x(n)x(n-l) + \frac{1}{N} \sum_{n=0}^{N-1} [x(n)w(n-l) + w(n)x(n-l)] + \frac{1}{N} \sum_{n=0}^{N-1} w(n)w(n-l) \\ &= R_{xx}(l) + R_{xw}(l) + R_{wx}(l) + R_{ww}(l) \quad \dots\dots\dots \end{aligned} \quad (15)$$

Here  $x(n)$  is a repetitive signal and its autocorrelation sequence has the same repetition of the signal containing relatively large peaks ( $l=0, K, 2K, \dots$ ). The cross correlation between the signal  $x(n)$  and non-repetitive noise  $w(n)$  is relatively small as both  $x(n)$  and  $w(n)$  are completely unrelated. The autocorrelation sequence of the random noise  $w(n)$  ( $R_{ww}(l)$ ) will contain a peak at  $l=0$ , but because of the random characteristics  $R_{ww}(l)$  decays rapidly towards zero. Hence  $R_{xx}(l)$  is the only term

expected to have large peaks for  $l > 0$ . Thus a repetitive signal  $x(n)$  buried in the random noise  $w(n)$  and its repetition rate can be identified using the autocorrelation function. Due to the presence of a finite data set of  $N$  samples, the amplitude of the peaks reduces as the shift  $l$  approaches  $N$ . Hence computing  $R_{yy}(l)$  was performed for  $l < N/2$  where  $N$  is the total number of data points [49].

### **3.2 Extraction of a signal using adaptive filtering**

Filtering techniques such as low pass, high pass and band pass filtering are commonly used if the signal and noise exist at different frequencies. Fixed single or multiple notch filters can also be used if the noise portion exists at fixed frequencies. In some biological signals, however, the signal and noise exist at the same frequency making conventional filtering techniques totally ineffective. Adaptive noise canceling works on the principle that a transfer function of a filter can be constantly changed to remove noise from a composite signal. By this technique a real physiologic signal can be extracted from a composite signal containing both noise and signal at the same frequency. Adaptive filtering requires a reference noise portion which is correlated only with the noise present in the composite signal. The reference need not be a representation of the signal, but must have a frequency spectrum similar to that of the noise portion of the composite signal.

Conventional filters such as low pass, band pass or high pass filters are linear and time-invariant. These filters perform a constant set of linear operations on a data sequence to provide an output based on the coefficient values. Adaptive filters do not have this restriction of time invariance. The filter parameters such as bandwidth and

resonant frequency change with time. The coefficients of the adaptive filters vary with time as they are adjusted automatically by an adaptive algorithm. Thus adaptive filters can be applied in a wide range of areas where the exact filtering operation required is unknown or in areas where conventional filters cannot be used [50].

An adaptive filter consists of a digital filter employed to perform the desired signal processing and an adaptive algorithm for adjusting the coefficients of that filter [51]. Fig. 5 is the block diagram of an adaptive filter.  $x(n)$  is the signal input into the digital filter, and  $y(n)$  is the corresponding output. The reference signal  $d(n)$  is extracted from the composite input signal  $x(n)$ , and the error  $e(n)$  is calculated as the difference between  $d(n)$  and  $y(n)$ . The coefficients of the digital filter are constantly adjusted by the adaptive algorithm to minimize the mean square value of  $e(n)$ . Thus the noise signal can be extracted from the composite signal if the reference noise signal is made available. The filter coefficients are updated so that the error is progressively minimized on a sample-by-sample basis [50].

The signal processing algorithm was designed such that the desired  $d(n)$  is the perfusion signal obtained at 810nm while  $x(n)$  is the input signal obtained from red or infrared source. The input signal contains both the perfusion signal as well as the oxygenation signal.

$$x(n) = oxy(n) + perf(n) \quad (16)$$

The adaptive filter extracts the perfusion signal  $perf(n)$  through output  $y(n)$  by iteratively minimizing the error between the primary ( $x(n)$ ) and reference inputs ( $d(n)$ ).

When convergence of the filter is achieved the filter output  $y(n)$  is the best estimate of the perfusion signal  $perf(n)$ .

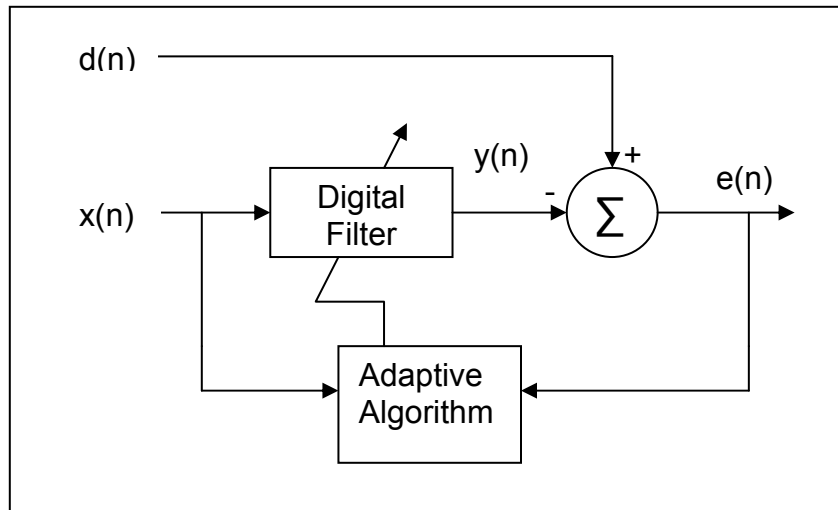


**Fig. 5.** Block diagram of adaptive filter

The digital filter computes the output in a linear fashion. Given a set of  $L$  filter coefficients,  $\{w_l(n), l = 0, 1, \dots, L-1\}$  and a data sequence,  $\{x(n), x(n-1), \dots, x(n-L+1)\}$ , the output signal is computed with the filter coefficients  $w_l(n)$ , which are time-varying and updated by the adaptive algorithm.

$$y(n) = \sum_{l=0}^{L-1} w_l(n)x(n-l) \quad (17)$$

The output signal in Eqn. 17 can be expressed by a vector operation. The system output  $y(n)$  is compared with the reference signal  $d(n)$  which results in the difference ( $e(n)$ ) signal (Eqn. 19):

$$y(n) = w^T(n)x(n) = x^T(n)w(n) \quad (18)$$

$$e(n) = d(n) - y(n) = d(n) - w^T(n)x(n) \quad (19)$$

The objective is to determine the weight vector so that the mean-square value of the error signal is minimized. This is done using a simple adaptive LMS algorithm, which does not require squaring, averaging, or differentiating [51]. The filter coefficients  $w_i(n)$ , obtained from the LMS algorithm are computed in Eqn. 20, where  $\mu$  is the step size of the filter. In this paper the LMS adaptive filtering algorithm was designed with a step size of ‘ $\mu=0.05$ ’ and order  $N=32$ . These values have been found to perform well in removing motion artifacts from pulse oximetry signals in previous publications [44].

$$w(n+1) = w(n) + \mu x(n)e(n) \quad (20)$$

As mentioned earlier, the signal obtained from the detector is the combination of both oxygenation ( $oxy(n)$ ) and perfusion ( $perf(n)$ ) signal. Once the perfusion signal is extracted from the original signal using adaptive filtering, the oxygenation signal can be reconstructed as follows,

$$x(n) = oxy(n) + perf(n) \quad (21)$$

$$oxy(n) = x(n) - perf(n) \quad (22)$$

The reconstructed oxygenation signal is further processed to obtain oxygen saturation information.

### 3.3 Multilayer Monte Carlo modeling of photon transport

Monte Carlo simulations have been widely used in Biomedical optics to simulate photon transport in tissues [52]. Lux *et al.* defined the Monte Carlo method as constructing a ‘stochastic model’ to determine the value of a physical quantity by



obtaining the expected value of a single or combination of random variables. Wilson and Adam first used the Monte Carlo technique in 1983 to model photon propagation through tissue [53]. Over the last twenty years the Monte Carlo simulations have gone through several improvements, the most popular being MCML (Monte Carlo – Multi Layer) by Wang *et al.* to simulate the photon transport in multiple layers [54]. The code was implemented in C programming language offering the advantage of portability in multiple computer platforms. The light transport in multi-layered structures can be visualized using Monte Carlo offering a simple and rigorous approach to measure multiple physical quantities simultaneously.

The technique involves launching a group of photons or photon packets into the medium whose absorption and scattering coefficients  $\mu_a$  and  $\mu_s$  respectively are specified by the user. The photons move a distance based on its mean free path and gets absorbed or scattered back based on the probability distribution function  $p(\chi)$  obtained from the computer generated random variable  $\xi$ .

Distance traveled by the photon, step size, is given as  $s = -\ln(1 - \xi)/\mu_t$  where,  $\mu_t$  is the total interaction coefficient which is the sum of the absorption and scattering coefficient.

Absorption effects reduce the weight of the photon packet while the scattering effect changes the propagation direction of a photon packet. A moving spherical coordinate system involving the deflection angle  $\theta$  and azimuthal angle  $\psi$  due to scattering are first sampled to obtain the direction change of the photon packet.

If  $W$  is the initial weight of the photon packet, then the fraction of photon weight  $\Delta W$ , absorbed can be calculated as,

$$\Delta W = (\mu_a/\mu_t) W \quad (23)$$

The weight of the photon is then updated ( $W=W-\Delta W$ ) and the propagation of photon is continued. In the case of scattering, the deflection angle  $\theta$  ( $0<\theta<\pi$ ) and azimuthal angle ( $0<\psi<2\pi$ ) are statistically sampled. The probability distribution of the cosine of the deflection angle,  $\cos \theta$ , is described by the scattering function originally proposed by Henyey – Greenstein [55] for galactic scattering.

$$p(\cos\theta) = (1-g^2) / (2(1+g^2-2g\cos\theta)^{3/2}) \quad (24)$$

where,  $g$  is the anisotropy which is equal to  $\langle \cos\theta \rangle$  and has a value between -1 and 1. Isotropic scattering and forward scattering are represented by the values of 0 and 1 respectively. Typical values of  $g$  range between 0.3 and 0.98 in tissues [56] but in the visible spectrum the value of  $g$  is  $\sim 0.9$ . The azimuthal angle is given by  $\psi = 2\pi\xi$ . The new direction of photon is calculated based on the deflection and azimuthal angles.

A photon packet undergoes series of absorption and scattering events after which the photon packet is terminated using a technique called Russian roulette [57] giving the photon packets one chance in  $k$  of surviving with a weight of  $kW$ . If the photon does not survive the photon weight is reduced to zero and hence terminated or is assigned additional weight when it survives the Russian roulette. The physical quantities such as photon reflectance, transmittance and absorption are recorded during the Monte Carlo simulation. A more complex method is involved in obtaining the physical quantities from a medium involving multiple layers. Data about these optical quantities and layer

changes are acquired in a multiple coordinate system. The user provides the absorption and scattering coefficients, refractive indices and thickness for each layer. Since light is a static entity the properties of the source are not required for many biomedical applications involving imaging and therapeutics [58].

A Multi layered Monte Carlo was designed by our group for multiple wavelengths to simulate photon transport in tissues to obtain the perfusion and oxygenation information. The simulation method adapted from an algorithm provided by McShane\* is described in the materials and methods section.

---

\* Private communication with Dr. Michael McShane, Assistant Professor, Louisiana Tech University, 2004

## CHAPTER IV

### MATERIALS AND METHODS

The first section of this chapter briefly describes the system design of the custom made sensor system. The second section explains the data simulation, *in vitro* and *in vivo* experimental setup used to verify the autocorrelation based time domain package. The final section covers the Monte Carlo data modeling and the experimental setup used in the real time separation of physiological signals using adaptive filtering. The signal processing package created using adaptive filtering is also explained in the final section.

#### **4.1 Sensor system design**

The sensor has been designed to measure perfusion of an organ by emitting light into the organ and detecting the backscattered light intensity. The current sensor system is designed to deliver three different wavelengths of light (660nm, 810nm and 940nm) to an area of tissue containing vessels in which the blood perfusion measurement can be taken. It is made up of three main components. The custom sensor probe head consists of a custom 4-in-1 diode, of which three slots were filled, allowing for independently modulated light sources to reside within one chip and therefore be projected into the same sample volume through the same spherical glass lens. All three LEDs were modulated at different frequencies around 2kHz via a custom designed unit developed by Oakridge National Laboratories (ORNL). The system operates similar to an RF system that modulates each of the LED wavelengths by a different carrier and then

demodulates the output of the photodetector to remove each of the carriers leaving the biological signal of interest.

At a distance of 3mm from the source diode is a glass coated silicon photodiode that measures 2mm square and is capable of detecting all three wavelengths simultaneously by frequency modulation. The probe head (Fig. 6) is tethered to a custom circuit box that consists of the diode power supply and frequency modulation circuitry as well as the signal collection circuitry.

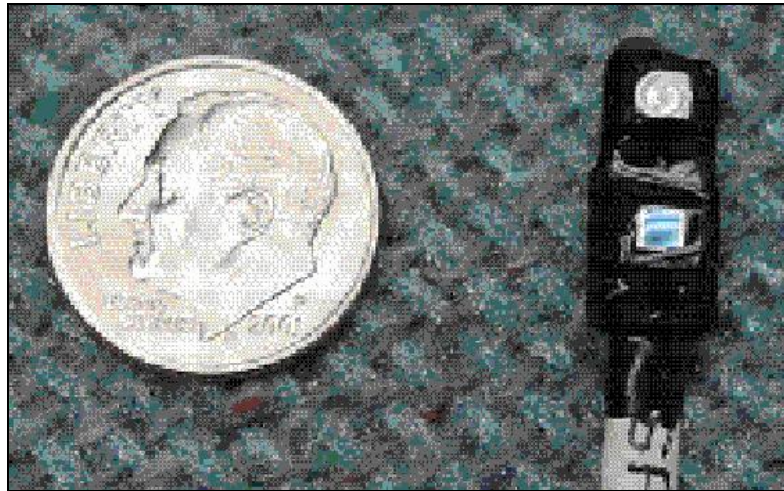


**Fig. 6.** Probe containing 3 different LEDs and a photodetector

The collection circuitry is made up of a frequency demodulation circuit and a series of analog filters for each of the three sources. The analog outputs from the sensor interface electronics are input to National Instruments data acquisition card located in the notebook PC PCMCIA slot. A LABView® (National Instruments) data acquisition program was written to collect the data in real time. The instrument also provides extra analog input channels that can be digitized with the sensor data. This provides a

convenient interface for collecting time-correlated data from other laboratory instruments that can be used during perfusion tests such as Laser Doppler flow meter.

The block diagram of the sensor drive and processing electronics is shown in Fig. 7, and the fabricated instrument is shown in Fig. 8.

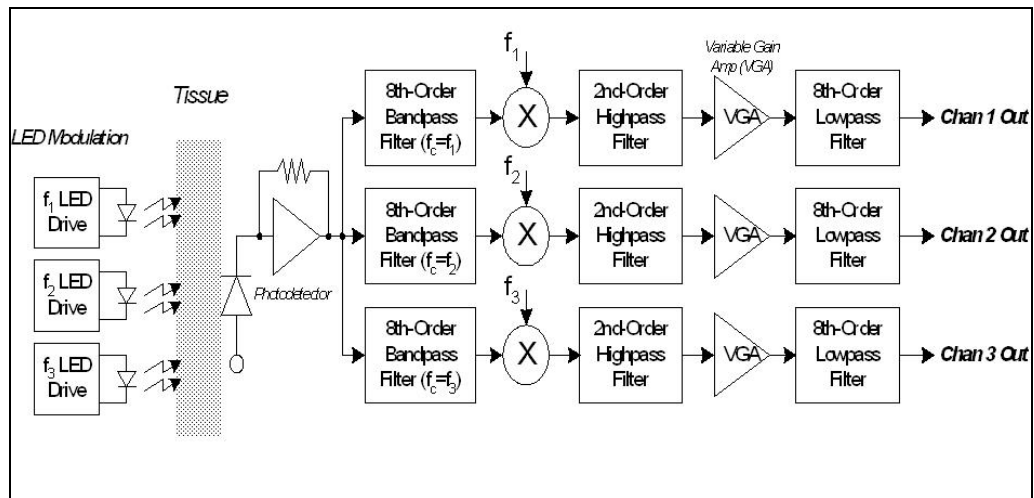


**Fig. 7.** Block diagram of sensor drive and processing electronics [4]

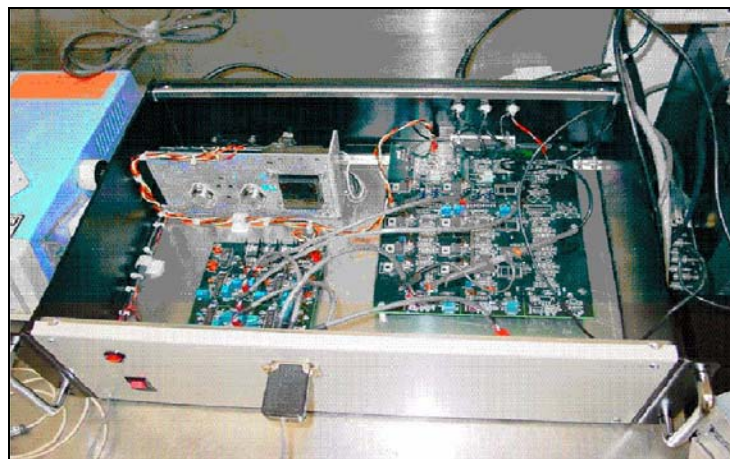


**Fig. 8.** Custom electronics for sensor interfacing and data collection [4]

## 4.2 Real time analysis of blood perfusion and oxygenation

### 4.2.1 Data simulation

A semi-periodic signal was generated that mimicked the perfusion and oxygenation signal commonly observed in the human body. The signal (*Datasimul.m* – Appendix A) was created by combining various sinusoids of different weights with a range of 2.95-3.05Hz using Matlab 5.3 (Mathworks, Inc). The central frequency was chosen randomly within this range and given a greater weighting. This frequency range was chosen because it is consistent with that observed in heart rate variability studies in pigs. The model data set was constructed using a sampling rate of 300Hz at a length of 50 seconds. High and low frequencies of random amplitudes were added to the model data set to simulate the affect of motion artifact and respiration. The simulated data was created in the likeness of the *in vivo* clamping study and thus the amplitude was varied to represent the trend due to arterial clamping seen in the actual *in vivo* study.

### 4.2.2 In vitro system

A model for blood perfusion through an organ was created using an adjustable peristaltic perfusion system in which the output tube was surrounded by 2 millimeter-thick chicken breast tissue that was perfused with a mixture of washed pooled bovine red blood cells with a buffer solution. An adjustable gas flow system was constructed so that the experimenter could alter the hemoglobin saturation by pumping in a set ratio of oxygen and nitrogen with fixed 5% carbon dioxide into the blood. The ratio between the gases was controlled so that certain  $sO_2$  levels could be reached and maintained. An adjustable peristaltic perfusion pump (MasterFlex L/S #7519-20, Cole-Parmer, IL), set at

4 Hz, pumped the gas treated bovine blood through the tissue-wrapped tube. The sensor described in section 4.1 was placed onto the surrounding tissue and mounted to limit motion artifact. Fifty-second segments of data were recorded three times at 300 samples per second for six separate oxygenation levels. The blood was then tested using a radiometer (Radiometer ABL 700 Series) to measure the true saturation level and chemical properties (pH, pO<sub>2</sub>, sO<sub>2</sub>, MeHb and CoHb). The *in vitro* data sets generated through the above procedure were analyzed using FFT and APAA methods similarly to the model data set.

#### 4.2.3 *In vivo* system

A female swine (50-60 kg) was given ketamine (10mg/kg) and xylazine (1.5mg/kg) for anesthetic induction and intubated under an approved animal use protocol. The pig was ventilated with 100% oxygen and anesthesia was maintained with inhalational isoflurane (1-4%). A Paratrend7 monitor (Diametrics Medical, Inc, MN) was placed on the left carotid artery via catheterized to allow for continuous blood gas analysis. Respiratory rate and tidal volume were adjusted to maintain PaCO<sub>2</sub> between 40–45 mmHg. The right femoral artery was cannulated with a Millar pressure transducer and a femoral catheter was inserted for blood sampling (Fig. 9).





**Fig. 9.** Setup for *in vivo* experiment

A Swan Ganz catheter was placed via the left internal jugular vein for cardiac output and mixed venous blood measurements. A laparotomy was performed and the pig was allowed one hour for stabilization. The sensor described in section 4.1 was placed on the serosal surface of the proximal jejunum and a clamp was applied to the vasculature supplying that region. A baseline signal was acquired for 50 seconds, four times prior to clamping of the vasculature. The clamp was then adjusted to three separate stages and data was acquired for 50 seconds, four times, at each stage. Finally, the clamp was removed and reperfusion data was collected the same way. Following the procedure, the animal was euthanized with a saturated solution of intravenous KCl (10 ml/kg) after the depth of anesthesia was increased with 5% isoflurane. The *in vivo* data set consisted of 20, 50-second data segments that represented the clamping procedure. These data segments were analyzed using the FFT and APAA methods similarly to the model data set.

#### 4.2.4 Signal processing

An autocorrelation-based perfusion analysis algorithm (APAA) was developed (*apaa.m* – Appendix B). Since the *in vivo* data sets contained both low and high frequency noise due to motion and respiration (Fig. 10a), the first process in this algorithm included the design of a digital band pass filter that limited the raw data to the physiologic range of interest (1-5 Hz, Porcine) (Fig. 10b). Secondly, autocorrelation was performed on the data segment resulting in a signal that contained peaks at intervals equal to the repetition rate of the original signal (Fig. 10c). A peak finding algorithm was used to detect adjacent peaks and calculate the repetition rate of the signal. From this repetition rate, the rate per minute (pulse rate) of the signal was obtained. A moving window with the width set to the pulse rate was then used to pick the maximum and minimum points from the filtered signal (Fig. 10d). The amplitude of the signal of interest was obtained by measuring the difference between the maximum and minimum points.

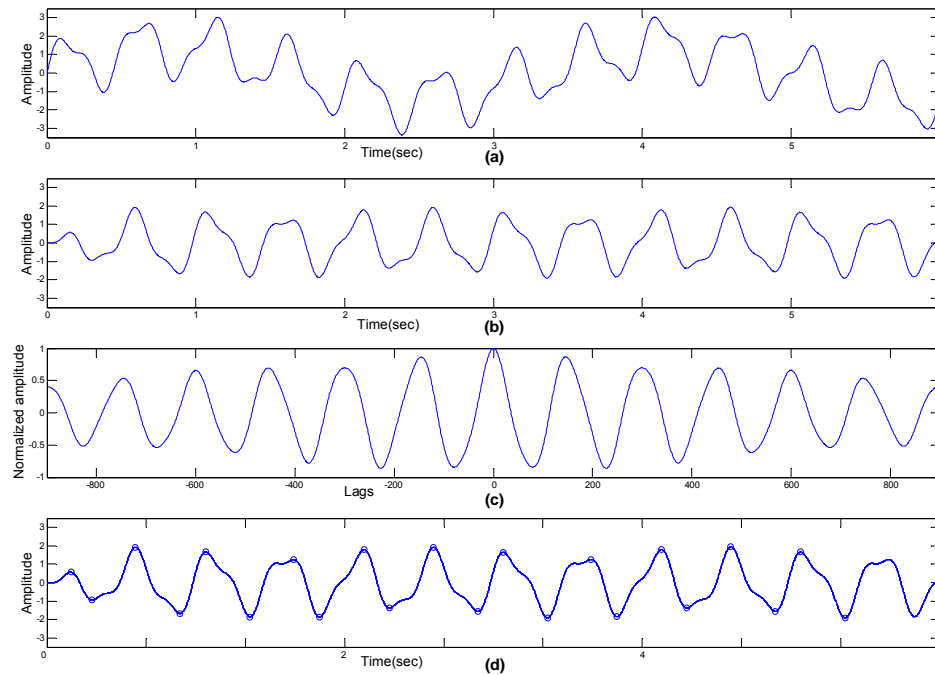


**Fig. 10.** Sketch of autocorrelation based perfusion analysis algorithm. (a) *in vivo* perfusion signal (b) the filtered signal (c) autocorrelated signal and (d) the result of peak finding algorithm

FFT and APAA processing methods were evaluated for all three data sets. Since the simulated data was created in the likeness of the *in vivo* clamping study, the amplitude was altered to represent the trend seen in the *in vivo* experiment. Both FFT and APAA processing techniques were subjected to similar filtering techniques to remove high and low frequency oscillations. The transient response of the digital band pass filter created an artifact in the first 2 seconds of the data that was not representative of the model, but rather the filter. To avoid error due to this response, the final data set was cropped to 48 seconds. The entire 48-second data set was used for full-segment analysis and further split into six equal segments of 8-second length and twelve equal

segments of 4-second length for short-segment analysis. The amplitude of the filtered signal was isolated using both FFT and APAA analysis. In order to obtain an AC amplitude for the FFT analysis, the spectral amplitude at the frequency of interest was divided by the number of data points in the signal. The average amplitude and standard deviation were calculated for all three data set lengths for both the FFT and APAA techniques. The APAA and FFT processing methods (*Simultanalyse.m* – Appendix C) were performed using Matlab 5.3 (Mathworks, Inc).

### **4.3 Separation of blood perfusion and oxygenation**

#### *4.3.1 Data simulation*

A data set was simulated to mimic the change seen due to oxygenation within a blood filled tissue. To simplify the model the physiology was broken down into five layers mimicking the *in vitro* setup. The first and last layers (2mm thick) were modeled using the optical properties of rat liver [59], similar to the tissue wrapped around the perfusion tube in the *in vitro* system. The second and fourth layers (2mm thick) were made non-scattering and non-absorbing and modeled as a slight increase in index of refraction as would be depicted in the *in vitro* clear plastic tube. The third layer (4mm thick) in the model is the whole blood layer mimicking what was pulsed through the tube in the *in vitro* perfusion system. It was assumed that the bulk of light absorption for the red and near-infrared regions in this layer was due to hemoglobin and therefore all absorptive values were based on the hemoglobin absorption spectrum. Scattering and anisotropy values were extrapolated for the wavelength range of 600-1000 nanometers

from published literature [60]. Table 1 shows the optical properties used for the various layers over the wavelength range of 600-1000 nanometers.

**Table 1:** Summary of the range of optical properties used for the model

<b>Tissue Layer</b>	<b>Index of Refraction(n)</b>	<b>Absorption Coefficient (<math>\mu_a</math>)</b>	<b>Scattering Coefficient (<math>\mu_s</math>)</b>	<b>Anisotropy (g)</b>
Layer 1 & 5	1.4	0.5-6.5 $\text{cm}^{-1}$	50-80 $\text{cm}^{-1}$	0.92-0.97
Layer 2 & 4	1.5	0	0	0
Layer 3	1.4	2-46 $\text{cm}^{-1}$	189-309 $\text{cm}^{-1}$	0.98-0.99

Using the five layer model, multi-layer Monte Carlo (MLMC) [54,8] photon tracing code was compiled for the wavelength range from 600-1000 nanometers every 10 nanometers. Weights were given to the original photon packets which correspond to the source spectrum. The optical properties of the third layer were then altered by changing the absorption coefficients to mimic that seen with changing oxygenation. This was done 8 times to generate data that spanned 30 to 100% oxygen saturation of hemoglobin. The recorded data for the model was a sum of the diffusely reflected light from 2 to 4 millimeters from the source to model the light as it would be collected by the detector. The total intensity from each wavelength was grouped with other wavelengths from the same diode source and added to create three distinct files. Lastly, for use in our signal processing package, the change in signal due to oxygenation was replicated (from 30% to 100% back to 30%) at a frequency of 4Hz for a span of 50 seconds resulting in a sinusoidal signal of 1200 data point length. To model a constant perfusion, a separate signal was generated with a frequency of 4Hz, amplitude of 1, and length of 1200 data

points. The oxygenation signals were then weighted (5%) and added to the perfusion signals (95%) to generate a composite signal which was then used in analysis of the adaptive filter algorithm. (*LMSadaptive.m* – Appendix D).

In order to validate the results provided by the *in vitro* experiments, the previous data simulation model was adapted to provide simulated data to compare to *in vitro* experimental data. The oxygenation values derived from the model were used separately to weight 4Hz sinusoidal signals of amplitude 1, resulting in 8 signals for each wavelength whose overall amplitude changed relative to oxygenation level. These signals were then recombined with unweighted 4Hz sinusoidal signals of the same frequency to simulate a constant perfusion. The result of these additions was 8 composite signals for each wavelength which modeled blood oxygenation change from 30-100%.

#### 4.3.2 Data collection

The *in vitro* experimental setup was similar to that used to test the autocorrelation package. In order to check the adaptive filtering technique at two different states of varying perfusion and varying oxygenation seen in the arteries two kinds of experiments were carried out. In the first set of experiments (*in vitro-I*) the oxygenation was lowered from 100% oxygen to 30% oxygen while the perfusion was kept constant. In the second set of experiments (*in vitro-II*) the perfusion of blood was increased to six different levels while the oxygen saturation of the blood was kept constant at approximately 98%.

*In vivo* data was collected to determine the effectiveness of the adaptive filtering algorithm. The data was collected using the serosal surface of the swine jejunum

performed under an approved animal use protocol. The procedure was the same as the *in vivo* experimental set up described for the autocorrelation package.

#### 4.3.3 Signal processing

An adaptive filter was designed based on a Least Mean Square (LMS) adaptive algorithm (*Separatesignal.m* – Appendix E). The reference signal at 810nm was used as a reference to extract the perfusion from a composite signal. The measured red and infrared signals are used as an input to the digital adaptive filter to extract the corresponding perfusion signals. The extracted signal may have an intensity more or less than the measured signal. This depends on the intensity of the reference signal (810nm) used. With knowledge of the perfusion signal amplitude present in the red and infrared wavelength, the corrected oxygenation signal can be reconstructed by stretching or compressing the measured signal in accordance with the extracted perfusion signal.

The adaptive filtering technique was employed to separate the composite signal into perfusion and oxygenation signals. A real time algorithm using an autocorrelation technique [7] was used to obtain the peak to peak intensities of the extracted perfusion and oxygenation signals at different wavelengths. Using the standard ratio described earlier the blood oxygenation value was then calculated and compared to the known blood oxygenation. The entire signal processing package was designed using Matlab 5.3 (Mathworks, Inc).

## CHAPTER V

### RESULTS AND DISCUSSION

The first section of this chapter presents the results of the autocorrelation based perfusion algorithm obtained from simulated, *in vitro* and *in vivo* data. The final section describes, in detail, the results of the adaptive filtering package used in the separation of perfusion and oxygenation signals obtained from the *in vitro* model data, *in vitro*, and *in vivo* experiments.

#### **5.1 Real time analysis of blood perfusion and oxygenation**

##### *5.1.1 Data simulation*

The FFT and APAA results for the simulated data are shown in Fig. 11a and Fig. 11b respectively. Twenty sets of simulation data were created in such a way that the amplitude of each group of four data sets was equal. These groups had a decrease followed by an increase in amplitude to mimic the *in vivo* perfusion data. It can be seen that the FFT predicts a different amplitude for 4-second (S.E = 0.07) and 8-second (S.E = 0.128) data sets with a significant standard deviation between the segments (Fig. 11a). This demonstrates the main limitation of the FFT approach, namely the loss of frequency resolution for a limited number of samples. The APAA technique (Fig. 11b) predicts the amplitude much more accurately (S.E = 0.005) than the FFT (S.E = 0.128) for the smaller data sets. Fig. 11b demonstrates that within any set of 3 that the mean amplitude obtained from the 4-second and 8-second data was equal with standard errors nearly equal to zero (S.E = 0.005).



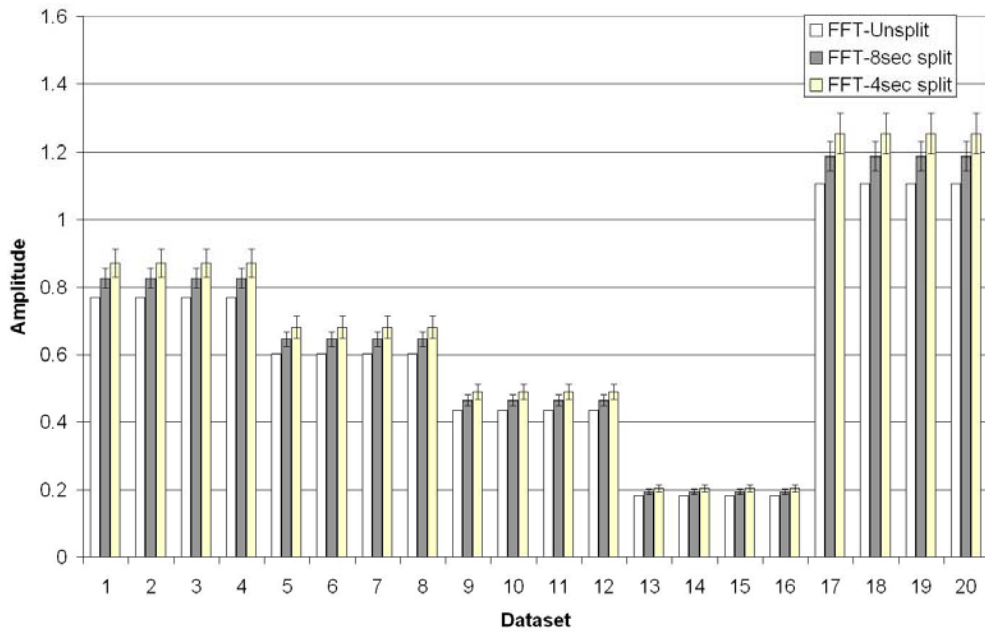


**Fig. 11a.** FFT results for simulated data in which perfusion signals mimic the *in vivo* data

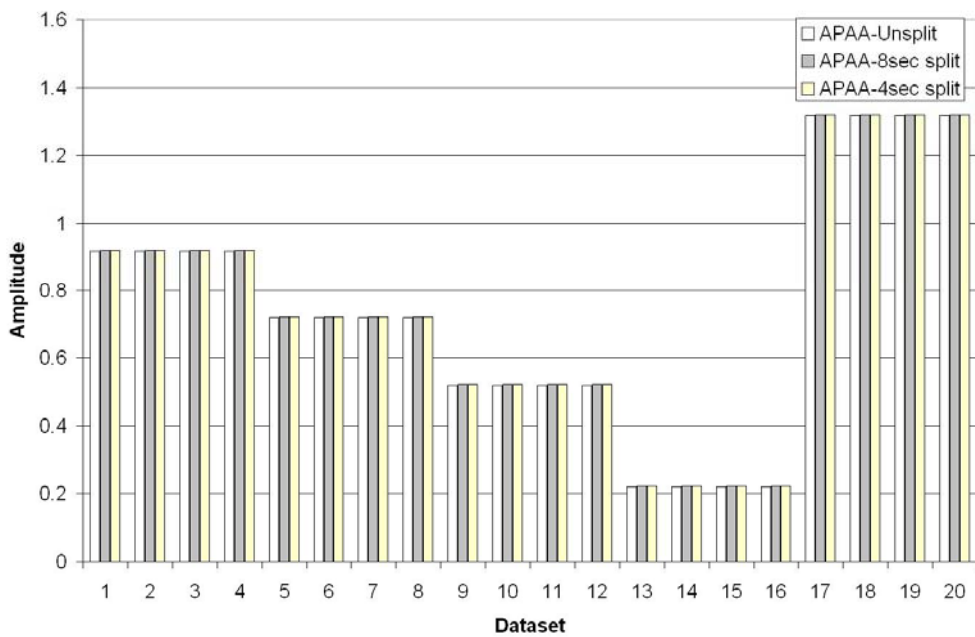


**Fig. 11b.** APAA results for simulated data in which perfusion signals mimic the *in vivo* data

Note that while the FFT signal in Fig. 11a varies for the 8 and 4sec data set, the APAA technique (Fig. 11b) is constant for the smaller data set since APAA adapts the window length according to the rate of the semi-periodic signal and unlike FFT does not suffer from the loss of frequency resolution for a limited number of samples.

### 5.1.2 *In vitro* study

The data from the *in vitro* experiment was also analyzed using both the FFT and APAA methods. Fig. 12 shows the raw data from the *in vitro* system containing a 4 Hertz signal with noise generated by the peristaltic pump. The autocorrelation signal obtained from the raw data is shown in Fig. 13. FFT analysis was performed on the raw data and a very sharp peak was seen at 4 Hz (Fig. 14). The oxygen saturation of the blood was changed from 4% to 100% by changing the gas ratio; the resulting oxygenation measurements from the Radiometer results are shown in Fig. 15.

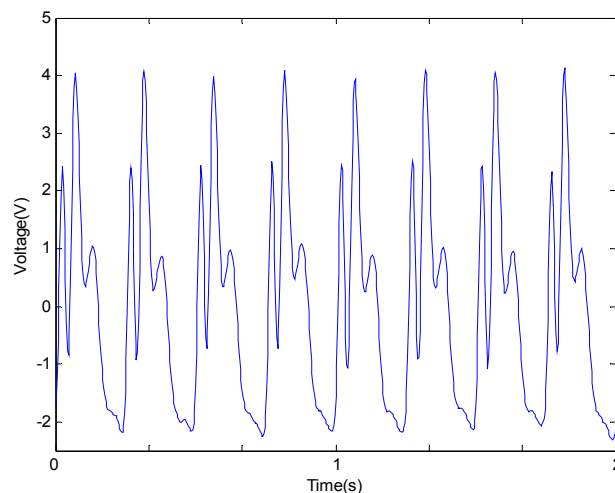


**Fig. 12.** Raw data from the *in vitro* system containing the 4Hz signal plus noise from the peristaltic pump

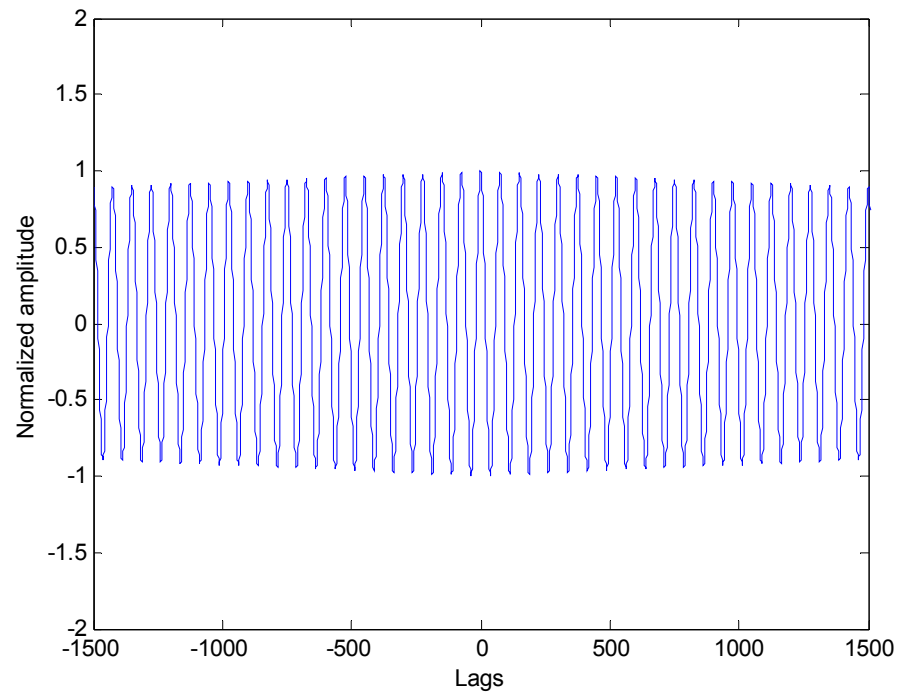


**Fig. 13.** Autocorrelation signal of the raw *in vitro* data

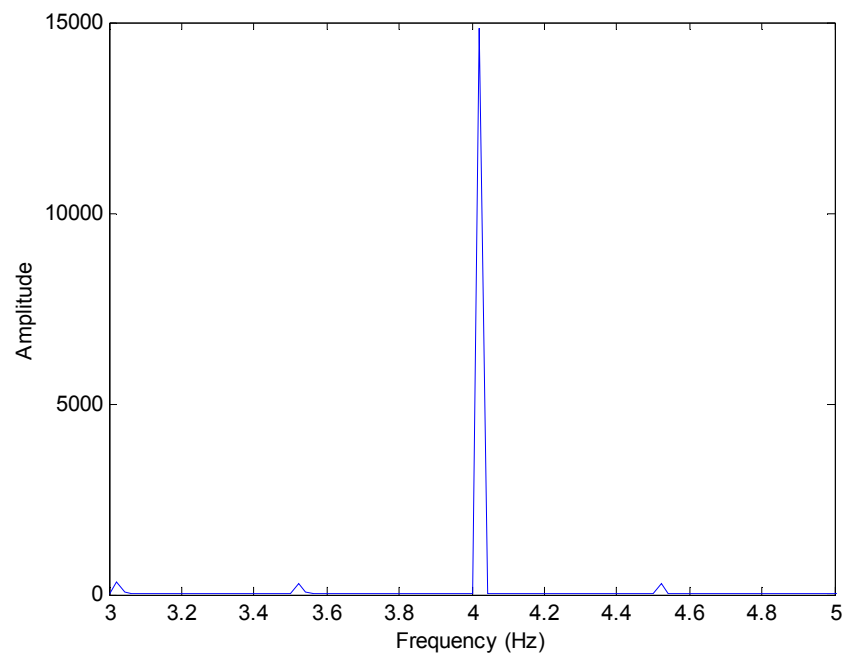


**Fig. 14.** FFT spectrum of the raw *in vitro* data

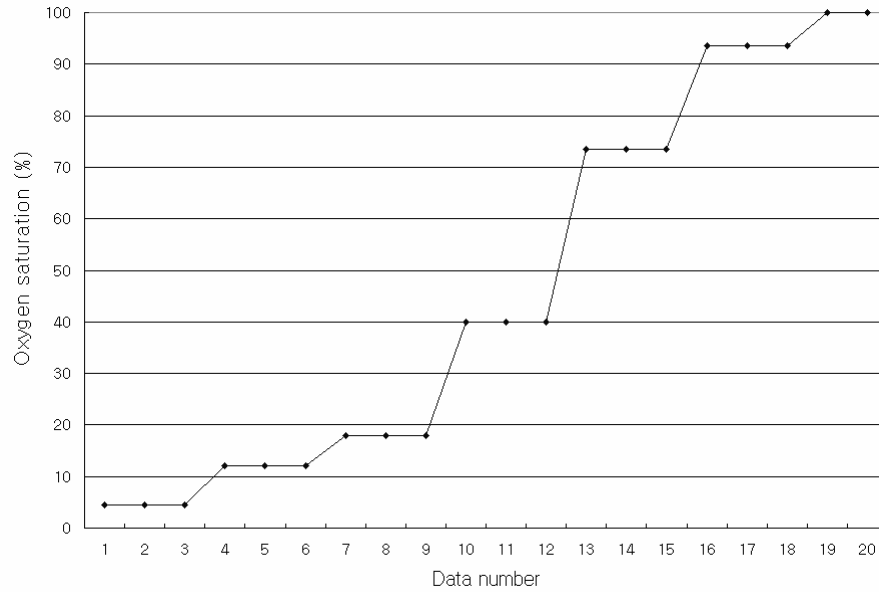


**Fig. 15:** Oxygen saturation from Radiometer

Both the FFT and APAA techniques were able to capture the change in absorption and showed only very slight differences in amplitude. The standard deviation (S.D = 0.003) of both data sets was small and the means across the same oxygenation states were relatively constant. Fig. 16a and Fig. 16b show that the 940nm source used in this sensor decreases in intensity with rising oxygenation, as predicted by the hemoglobin absorbance spectra [10]. The other two sources showed comparable results and were therefore not shown. From this analysis it can be seen that little difference exists between the APAA technique and standard FFT analysis when the raw data is periodic.

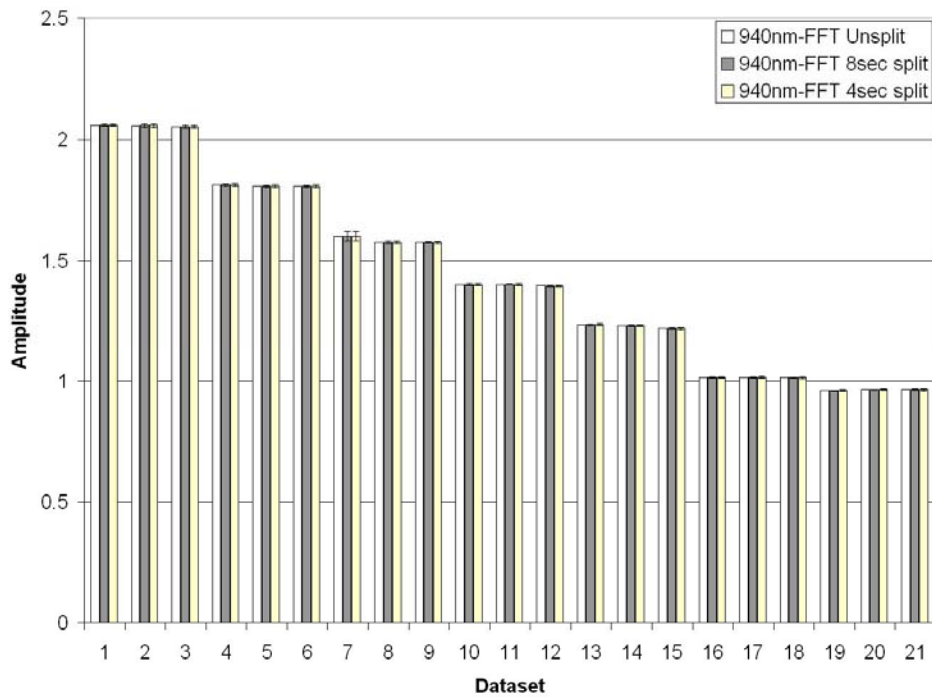


**Fig. 16a.** FFT results for *in vitro* data showing constant means across 8sec and 4sec split with same blood oxygenation states

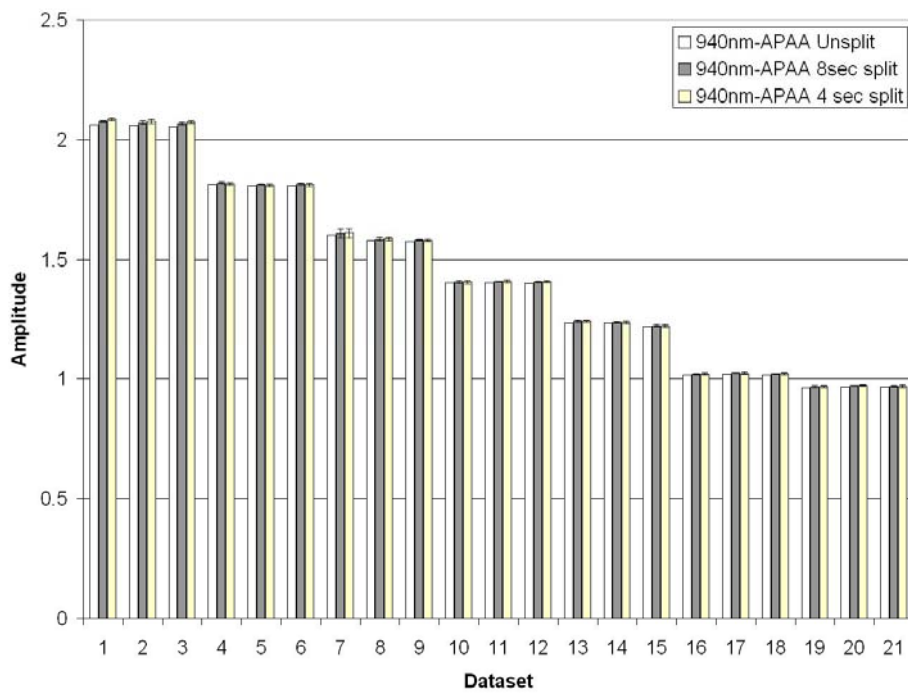


**Fig. 16b.** APAA results for *in vitro* data showing constant means across 8sec and 4sec split with same blood oxygenation states

### 5.1.3 *In vivo* study

The amplitude of the *in vivo* perfusion signal was calculated using both the FFT and APAA algorithms as shown in Fig. 17- Fig. 19 for each of three sensor sources. The experimental protocol used a graduated clamping procedure to change the overall perfusion of the monitored organ. This protocol differs from the *in vitro* data set in that the perfusion was changed rather than the oxygen saturation of the blood. This however does not affect the analysis technique because both of these phenomena occur at the same frequency. The notable difference is that the three sources will change in the same fashion under a perfusion change (volume dependent) whereas an oxygenation change will affect the sources differently as it is dependent on the hemoglobin absorption characteristics [10].

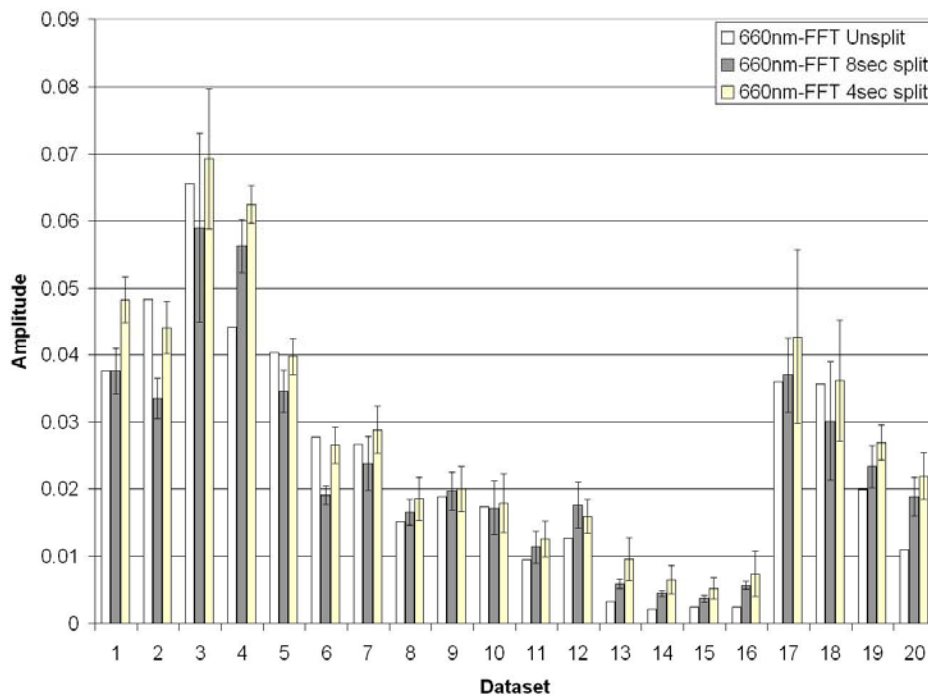


**Fig. 17a.** FFT results for *in vivo* data (660nm source) showing inconsistent means across 8sec and 4sec split with same blood perfusion states

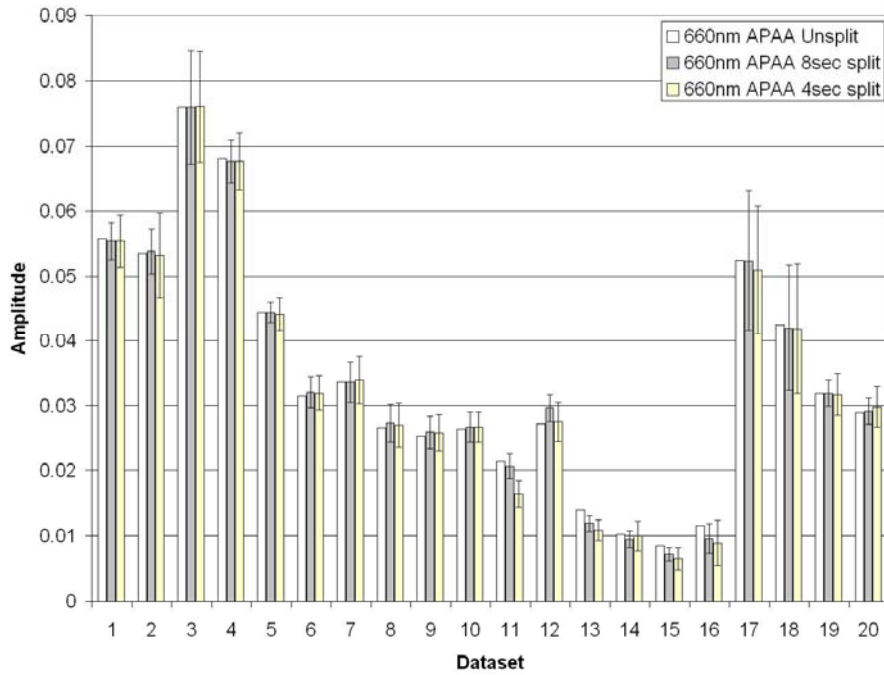


**Fig. 17b.** APAA results for *in vivo* data (660nm source) showing constant means across 8sec and 4sec split with same blood perfusion states

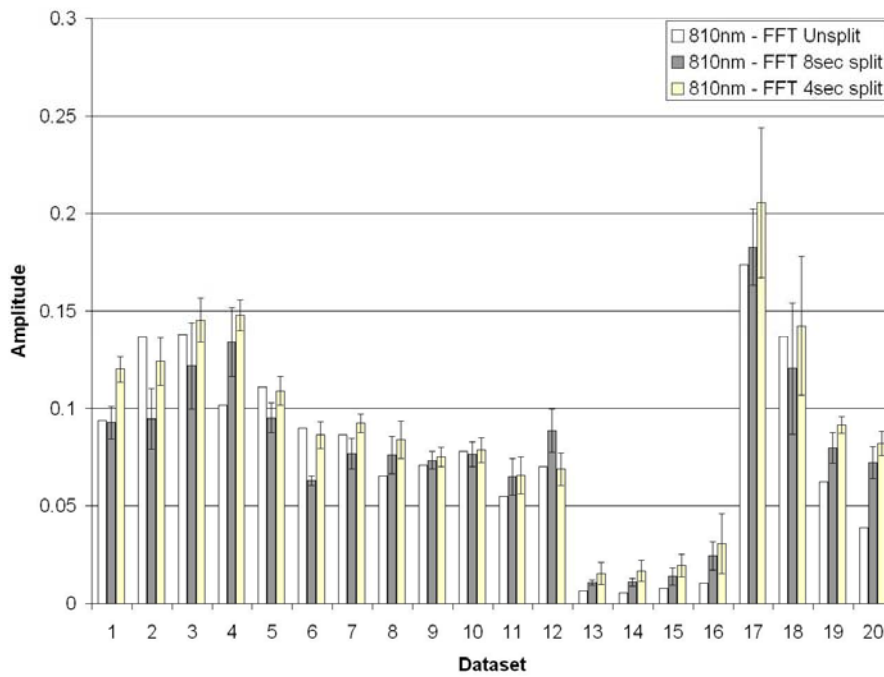


**Fig. 18a.** FFT results for *in vivo* data (810nm source) showing inconsistent means across 8sec and 4sec split with same blood perfusion states

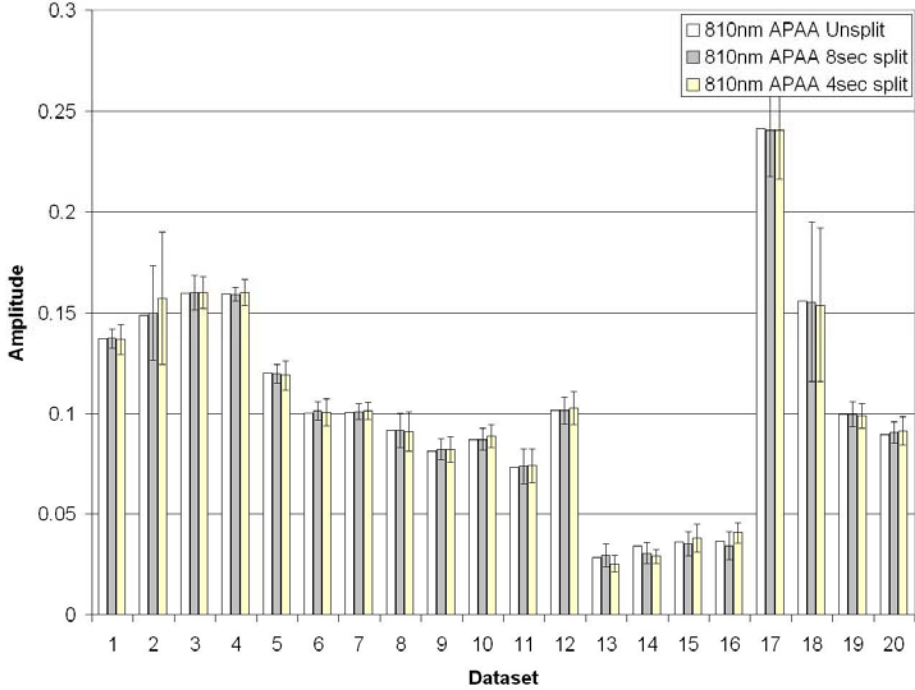


**Fig. 18b.** APAA results for *in vivo* data (810nm source) showing constant means across 8sec and 4sec split with same blood perfusion states

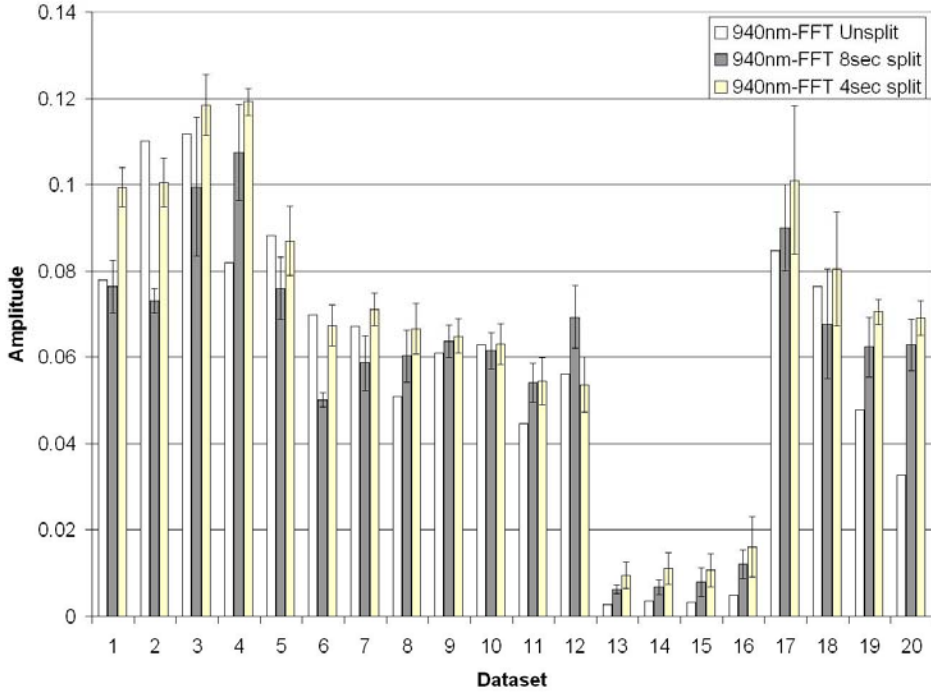


**Fig. 19a.** FFT results for *in vivo* data (940nm source) showing inconsistent means across 8sec and 4sec split with same blood perfusion states



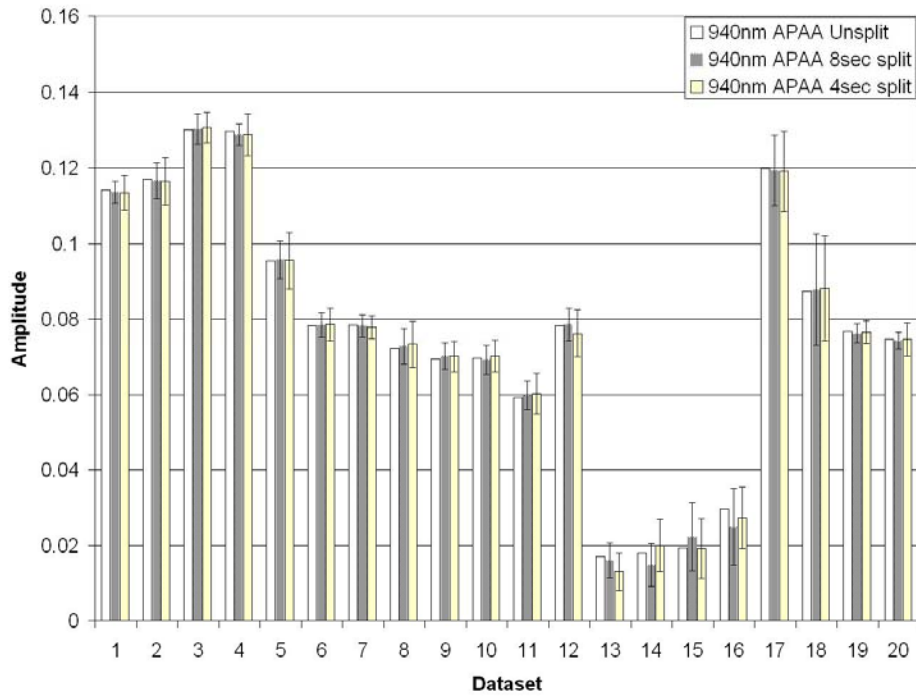


**Fig. 19b.** APAA results for *in vivo* data (940nm source) showing constant means across 8sec and 4sec split with same blood perfusion states

The APAA method showed the estimated amplitudes of the filtered 48-second data, the average of 8-second data, and the average of the 4-second data to be nearly equivalent per wavelength as depicted in the Fig. 17b, 18b, and 19b. Variations in amplitude between the wavelengths are due to differences in penetration depth, sensor position, and differences in source output intensities. The FFT analysis of the same data showed estimated peak amplitude fluctuations of the 48-second, 8-second, and 4-second segments to be greater than the APAA technique (Fig. 17a, 18a, and 19a). It can be seen that the APAA technique is much more consistent over the three segment lengths showing less amplitude variation and a smaller standard deviation on average (Table 2). This difference can be attributed to the *in vivo* signal being semi-periodic. Semi-

periodicity causes the FFT spectrum for the filtered 48-second signal (Fig. 20) to become broad with a large frequency distribution around the frequency of interest compared to the FFT spectrum of *in vitro* data (Fig. 14). When the data is shortened from 48 to 8 seconds, a loss of resolution is depicted due to a limited sampling rate, which results in less accurate amplitude estimates. In order to counteract this effect the sampling rate needs to be increased but this would result in a slower and less efficient system.

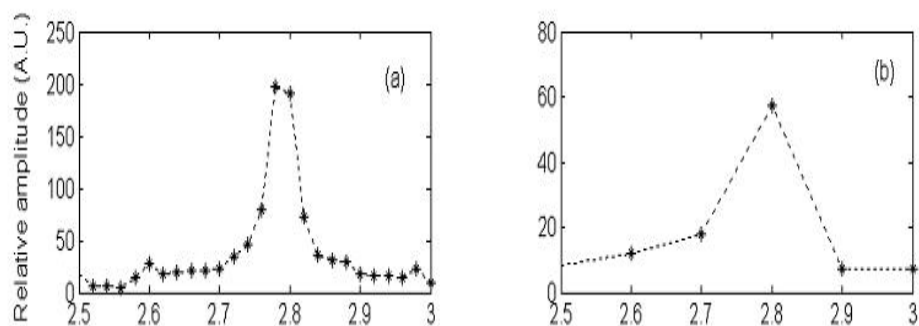


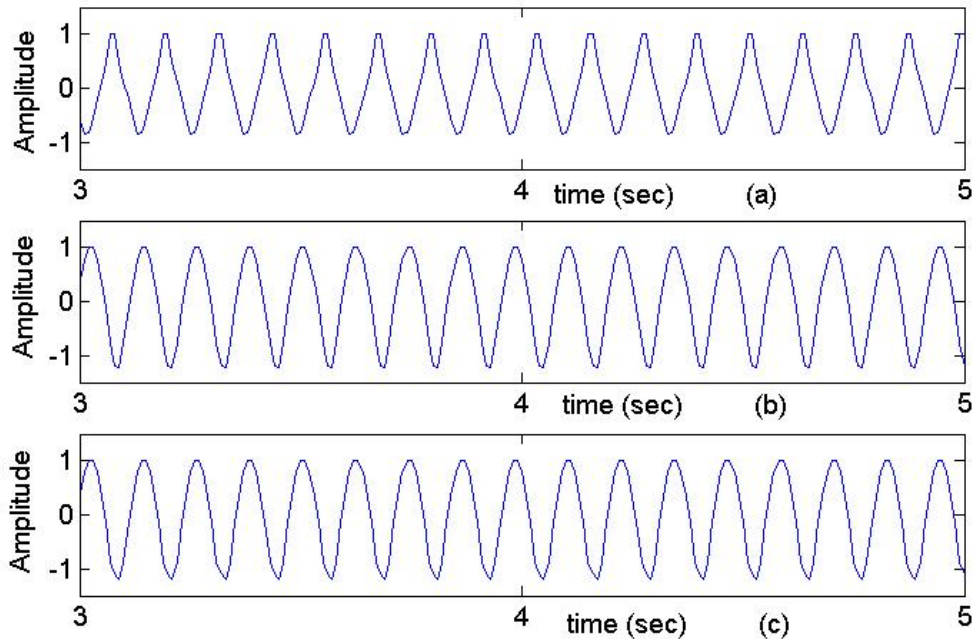
**Fig. 20.** An example of the FFT spectrum obtained. (a) using 48 seconds of data and (b) using spectra of 8-second data from the 660 nm signal of *in vivo* experiment

**Table 2:** Summary of the standard error calculated against un-split data

	Simulated data		<i>In vitro</i> data		<i>In vivo</i> data	
	8-sec split	4-sec split	8-sec split	4-sec split	8-sec split	4-sec split
FFT	0.070	0.128	0.0003	0.0003	0.417	0.616
APAA	0.005	0.006	0.004	0.004	0.032	0.029

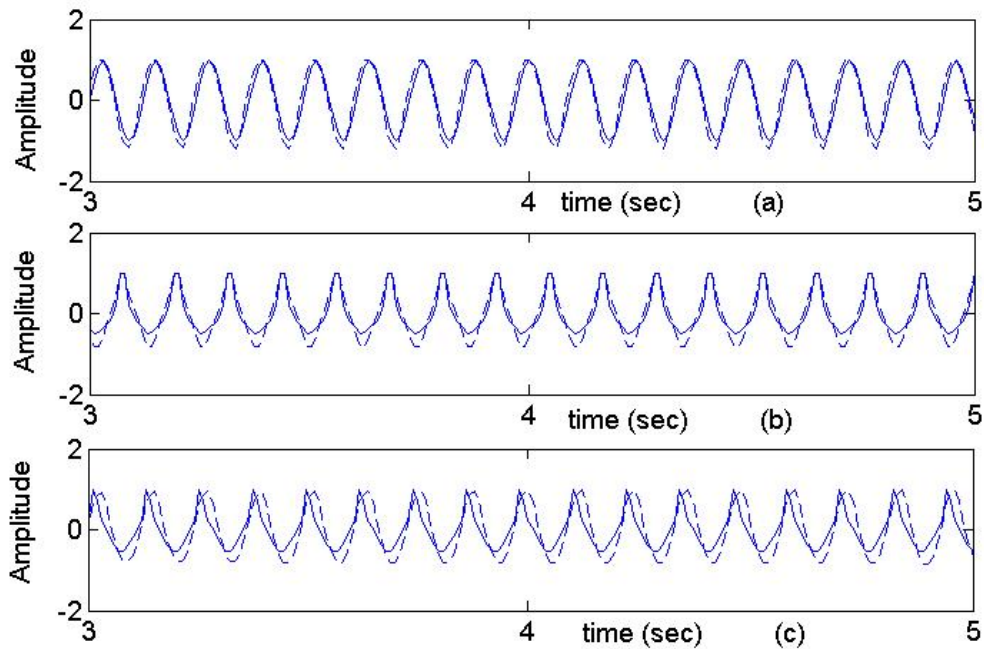
## 5.2 Separation of blood perfusion and oxygenation

The adaptive filter package was originally tested using data derived from a layered Monte Carlo model. The data derived from this model was based on the *in vitro* experimental setup, but designed to generate data as it would be seen *in vivo*. In a perfused organ two competing phenomena will affect the light returning to the sensor probe; change in perfusion and change in hemoglobin saturation. As blood enters the sampling volume it carries with it a slight increase in volume due to the pulse pressure and also a fresh amount of oxygenated hemoglobin for delivery to tissue. In order to model the two competing phenomenon, values similar to what would be expected physiologically must be generated. Using the described model, oxygenation values were generated that represent approximately what would be measured in a transplant organ with our sensor. In order to form a composite signal, a simple sinusoidal signal was generated and added to the oxygenation signal. This sinusoid modeled the increased volume that would be present in a pulsatile system (perfusion). The two signals were added at a ratio of 95% perfusion to 5% oxygenation to mimic a highly perfused region of tissue.



**Fig. 21.** Combined oxygenation and perfusion signal using Monte Carlo simulation.  
 (a) 660nm (b) 810nm and (c) 940nm

The composite signal is shown normalized in Fig. 21 for each of the three sources. The adaptive filtering algorithm was used to generate perfusion and oxygenation signals for the 660nm and 940nm wavelengths from these composite signals. The generated signals are shown in Fig. 22 as compared to the original independent signals derived from the Monte Carlo model. The perfusion signals for the two wavelengths match very well due to their large weighting in the composite signal. The infrared (940nm) perfusion signal is shown in Fig. 22a.



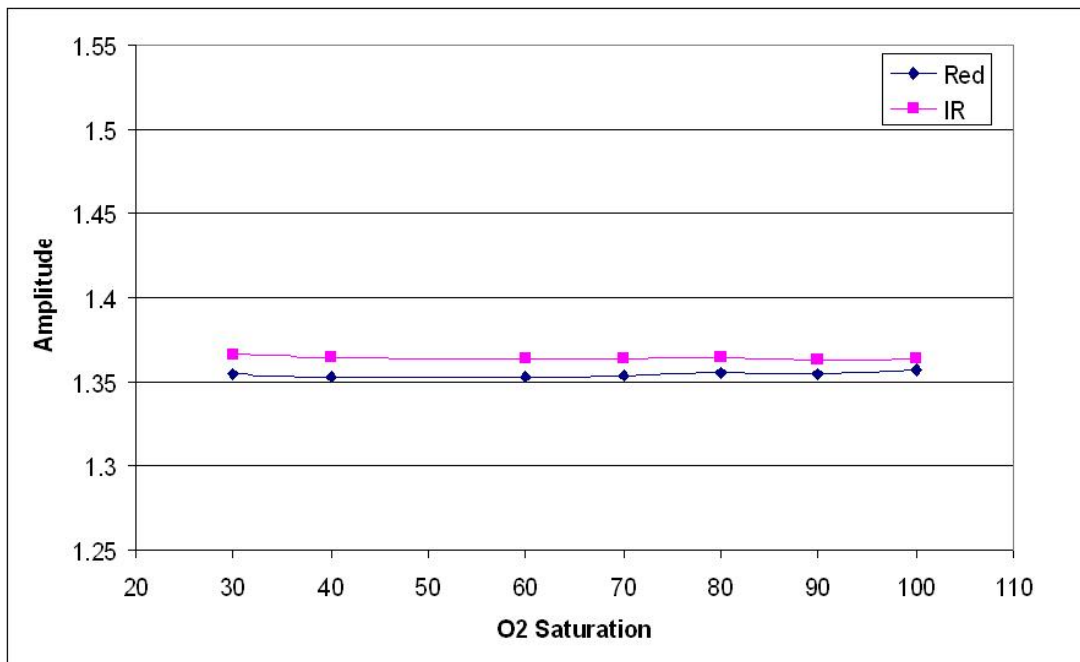
**Fig. 22.** Output signals from adaptive filter algorithm. (a) 940nm perfusion signal (b) 660nm oxygenation signal and (c) 940nm oxygenation signal

Fig. 22b and Fig. 22c show the extracted signals due to oxygenation for both red (660nm) and infrared (940nm) wavelengths. The solid lines depict the original pure signal and the dashed lines display the signal extracted through adaptive filtering. It can be seen that the signals appear different in shape due to the repetitive construction of the Monte Carlo derived data points and smoothing effect of the adaptive filtering. However, the amplitude and frequency of the signals is equivalent with error between the two of 0.01% in frequency and 0.2% in amplitude proving that the adaptive algorithm was able to extract oxygenation derived signal adequately. Also, it is important to note the phase between the red (660nm) and infrared (940nm) signals is shifted 180 degrees. This change in phase shows that this processing method accurately

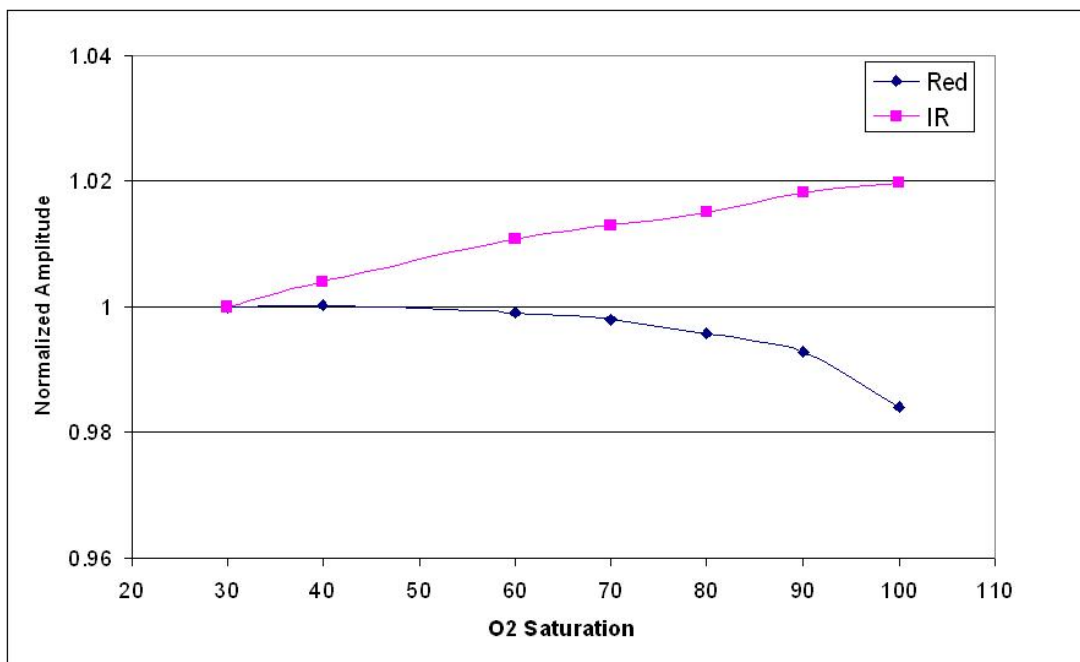
extracted the oxygenation signal because this phase difference is predicted from the hemoglobin absorption curve around the isosbestic point (810nm).

The *in vitro* experimental setup was created to measure the ability of the sensor to work in a more realistic setting containing motion artifacts and system noise. As stated earlier the pump modulation frequency is seen as the heart pulse signal, but is independent of volume changes due to a rigid tube and also oxygenation due to lack of a chemical reaction within the sampling volume. To change these parameters two things were done; the volume per pulse was changed via a larger bore pumping tube and the oxygenation was changed externally to a chosen level via gas interaction. This means that data segments exist at a single set oxygenation or a single set perfusion level for an entire 50 second data set. Therefore the resulting data consisted of multiple 50 second segments each of which being a constant perfusion value with a constant oxygenation state. By combining these files into one large continuous data set, a composite signal can be formed which contains either a perfusion change or saturation change.

The first *in vitro* data set was generated to show the sensor's response to changes in oxygenation within whole blood. Through the addition of ten files, 50 seconds in length, for each wavelength, a composite signal was made and the adaptive algorithm was performed. Fig. 23 shows the extracted perfusion signal from the first model data. As expected, through the use of a constant perfusion signal, the extracted signal is nearly constant. The extracted oxygenation signal as predicted by the Monte Carlo code versus oxygen saturation is shown in Fig. 24.

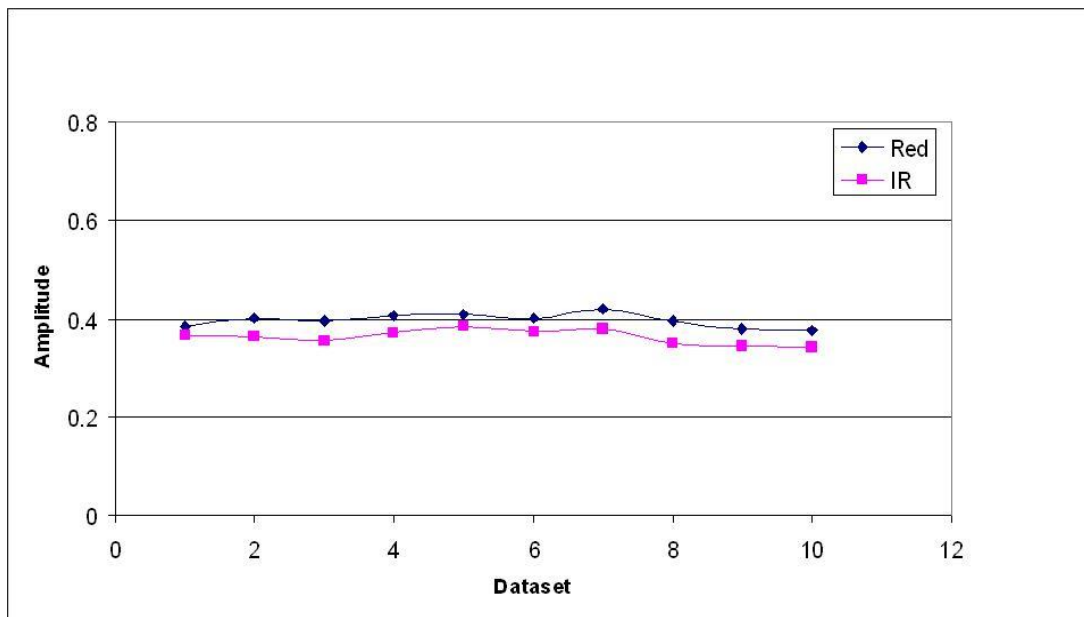


**Fig. 23.** Perfusion signal extracted from first Monte Carlo model data. As depicted the perfusion is pulled out as a constant even though oxygenation is varying



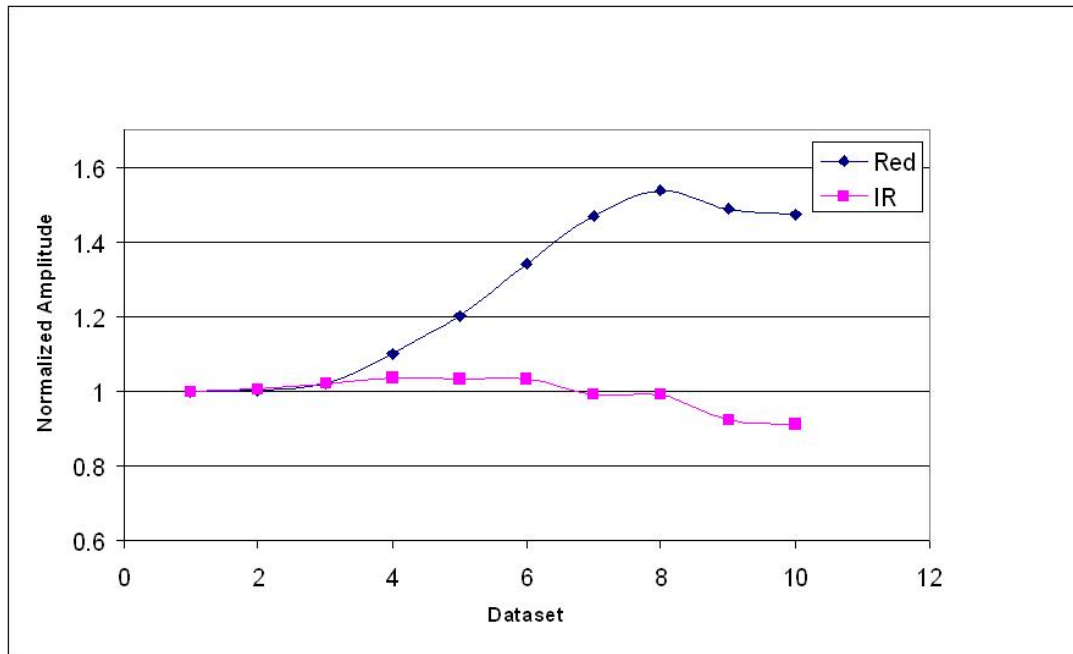
**Fig. 24.** Oxygenation signal extracted from first Monte Carlo model data. As depicted the oxygenation varies while the perfusion is constant

Fig. 25 and Fig. 26 show the two outputs for the red (660nm) and infrared (940nm) wavelengths for perfusion and oxygen saturation. What is seen is that perfusion was kept relatively constant by the rigid tube and the varying oxygenation from the gas exchanger caused changes in the signal. Fig. 24 and Fig. 26 compare very well showing that not only is the sensor able to detect the change due to oxygenation, but also that the adaptive algorithm successfully separated perfusion and oxygenation signals. Using the autocorrelation algorithm the oxygen saturation ratio was calculated and plotted against the known values (Fig. 27). It is seen that with decreasing oxygenation the ratio goes up, agreeing well with what is reported in literature [11], [21]. This graph was generated from four independent experiments using the same procedure, showing that this data is very consistent with standard error less than 2%.



**Fig. 25.** Perfusion signal extracted from first *in vitro* experiment showing constant perfusion signal while the oxygenation is varying





**Fig. 26.** Oxygenation signal extracted from first *in vitro* experiment showing varying oxygenation signal while the perfusion is constant

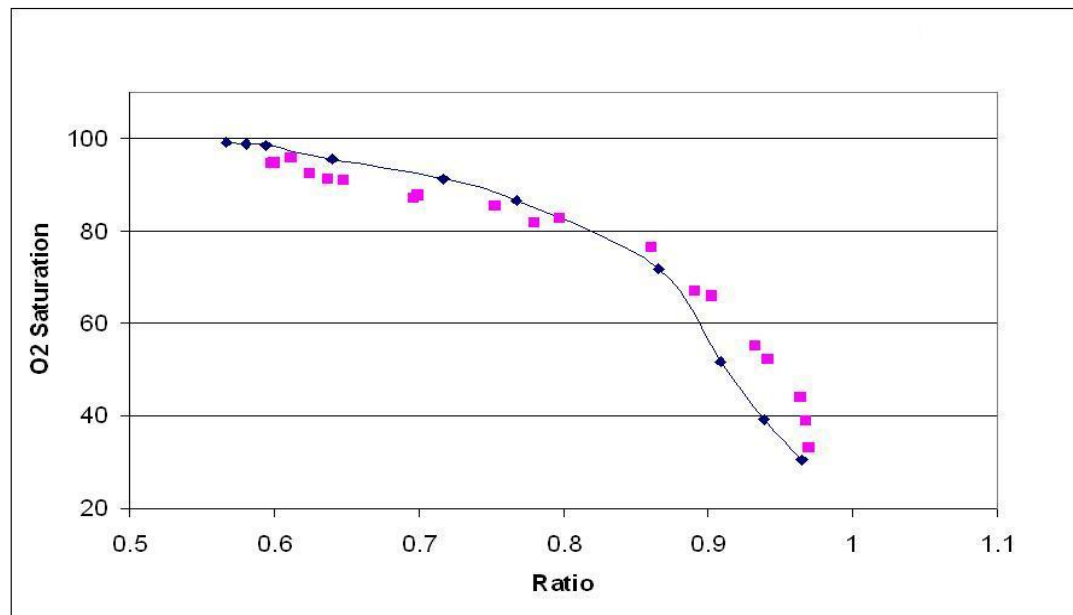


**Fig. 27.** Oxygenation ratio obtained from first *in vitro* experiment showing increasing oxygenation ratio with decreasing oxygen saturation

The second *in vitro* data set was created to determine if the sensor could perform well with changing perfusion. The experimental protocol consisted of increasing the bore size of the peristaltic tubing to cause a greater flow of fluid to pass through the sampling region per pulse. Fig. 28 shows the results from the adaptive filtering algorithm. This increase in flow appears as a rise in signal for the two wavelengths. This is due to an influx of absorbing material with each pulse that is greater depending on the pressure behind the fluid. This would generate greater absorbance in all the sources and manifest itself as an increase in the AC signal measured due to a bigger difference between the two oscillating states (pulse and rest). As expected, the perfusion signal changes in response to the increased flow. Also of importance is that the oxygenation signals (Fig. 29) trace each other with no noticeable deviations. This would translate into a ratio that is approximately the same across all data files. As expected, using the autocorrelation procedure, the resultant change in oxygenation is approximately zero as shown in Fig. 30.

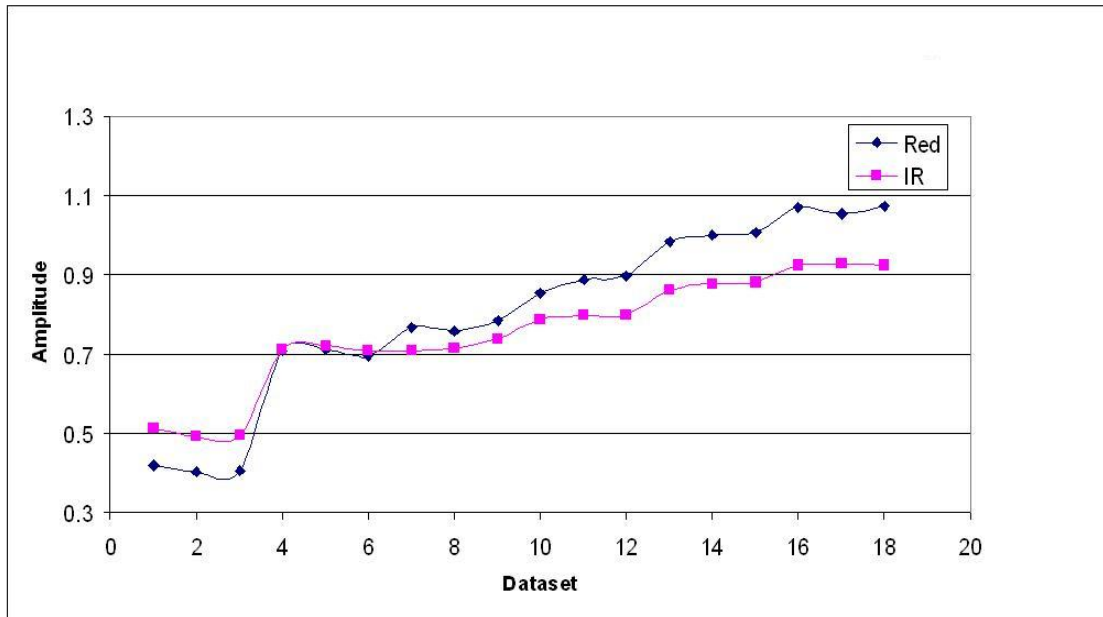


**Fig. 28.** Perfusion signal extracted from second *in vitro* experiment showing increasing perfusion while the oxygenation is constant

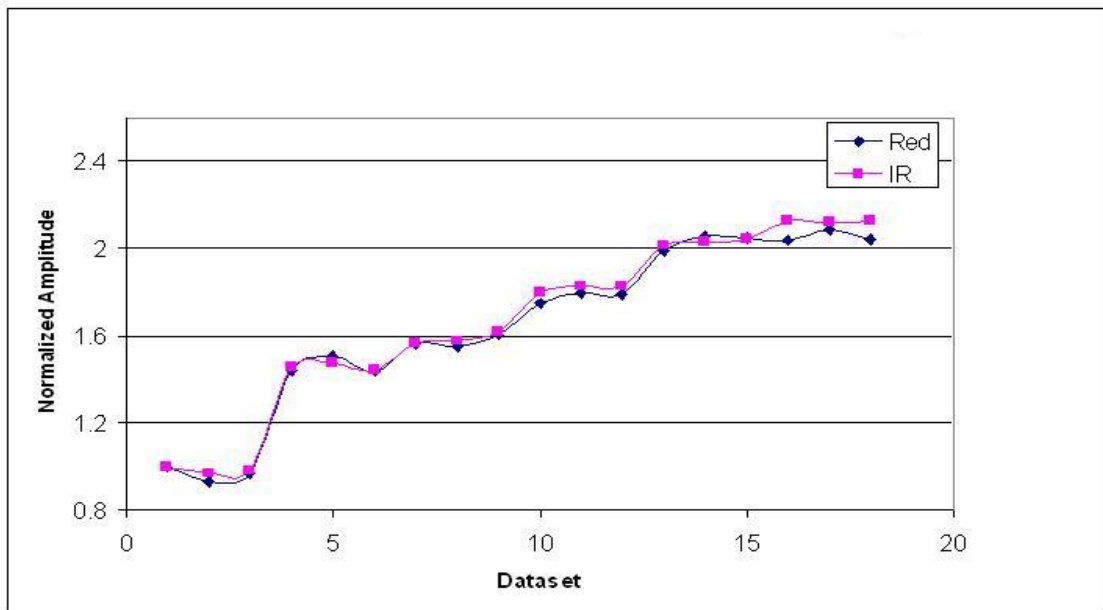


**Fig. 29.** Oxygenation signal extracted from second *in vitro* experiment showing increasing oxygenation with constant ratio

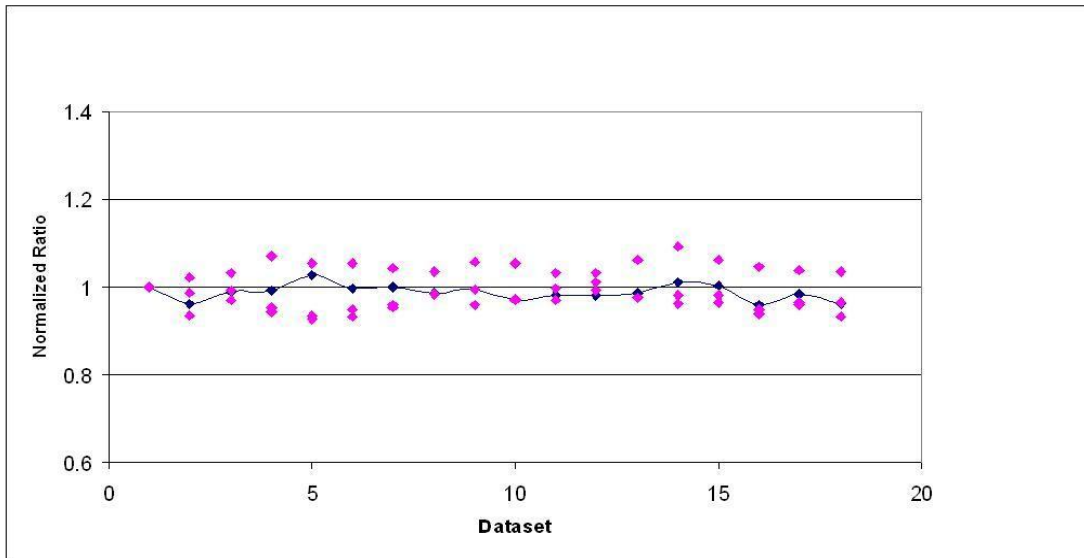


**Fig. 30.** Oxygenation ratio obtained from second *in vitro* experiment showing constant oxygenation ratio while the perfusion is varying

The last experimental setup was performed by placing the sensor on the surface of a swine intestine. The mesentery arteries were then systematically clamped to induce a large perfusion change in the illuminated tissue. The sensor recorded four, 50 second data segments for each of the 5 stages. Fig. 31 and Fig. 32 show the extracted perfusion and oxygenation signals as seen after the adaptive filtering. The noticeable drop seen in the signal for each of the first four stages is due to the clamping of the arteries and the drastic rise in the last stage is due to the hyperemic response of the tissue upon reperfusion. The oxygenation signal (Fig. 33) shows a near constant oxygen saturation ratio until the point where all blood is cut off (File 13). The total loss of perfusion manifests itself electronically as a complete loss of the main pulsatile frequency causing error in the adaptive filtering and autocorrelation algorithms. Upon reperfusion, however, the pulsatile nature of the signal returns and the system regains its prior oxygen

saturation consistency. This experiment shows the ability of this sensor to perform both a perfusion measurement and calculate relative oxygen saturation values in low blood flow states, but clearly yields false results for oxygenation when there is no flow.

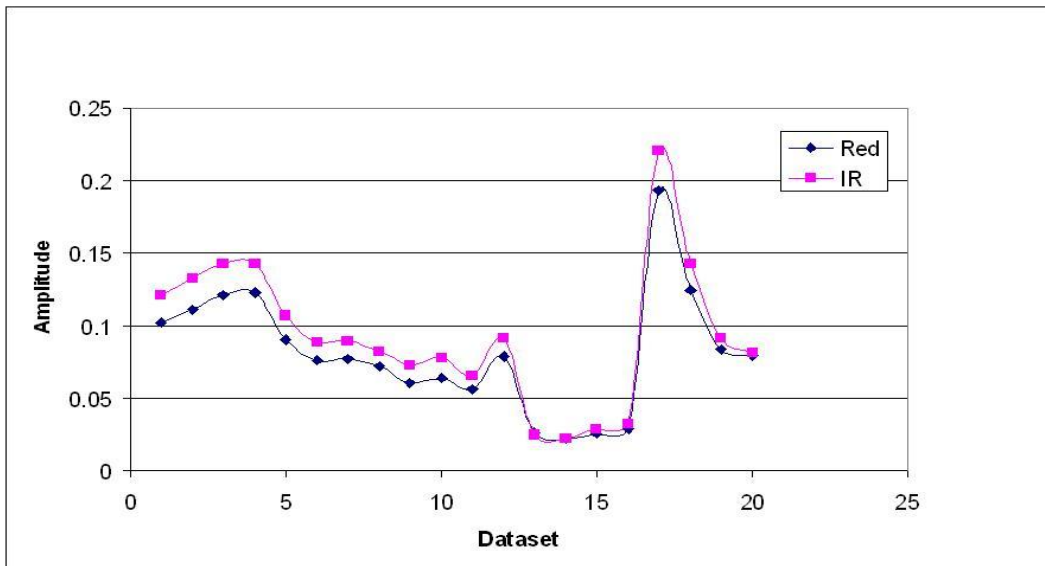


**Fig. 31.** Perfusion signal extracted from *in vivo* experiment showing decreasing perfusion state during clamp stage and increasing perfusion in reperfusion stage

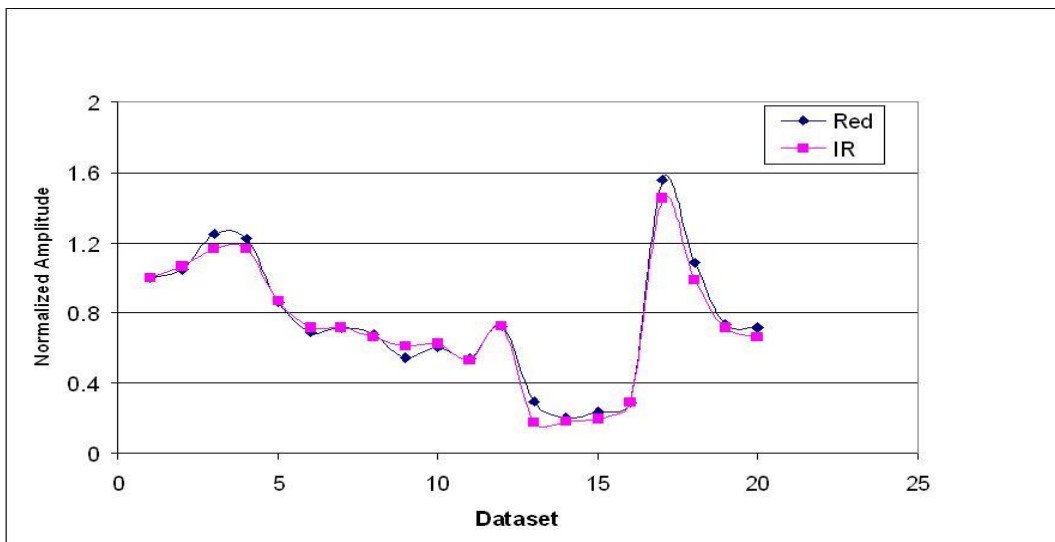


**Fig. 32.** Oxygenation signal extracted from *in vivo* experiment showing decreasing oxygenation with a constant ratio between 660nm and 940nm source

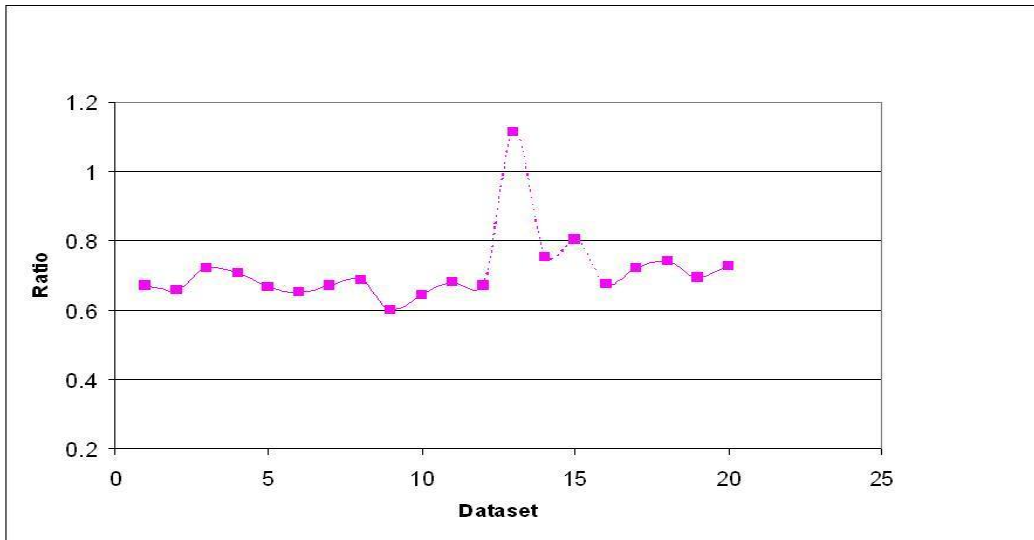


**Fig. 33.** Oxygenation ratio obtained from *in vivo* experiment showing constant oxygenation ratio with varying perfusion

The adaptive filtering technique primarily separates the perfusion signal and oxygenation signal from the composite signal obtained by the detector. In traditional oximeters, the perfusion information is obtained in the form of a plethysmograph signal using a single wavelength. The oxygenation ratio thus obtained would be the combination of both the perfusion signal and the oxygenation information. This is critical in situations where the perfusion signal is widely fluctuating. The adaptive filtering technique proposed here can be used in these circumstances to separate the perfusion signal and obtain more robust oxygenation information. As shown in Fig. 34, the oxygenation ratio obtained without the adaptive filter is similar to that obtained by using adaptive filtering in the *in vitro* experiment. This is the situation experienced in healthy patients (near constant perfusion). But in patients experiencing low blood perfusion the oxygenation ratio fluctuates thus yielding incorrect arterial oxygen saturation values. This situation is similar to the *in vivo* (Fig. 35) experiment where the

oxygenation ratio fluctuates more than those obtained using adaptive filtering. Even though slight variation can be seen after adaptive filtering, the ratio obtained with the combined algorithm is more stable than autocorrelation alone.

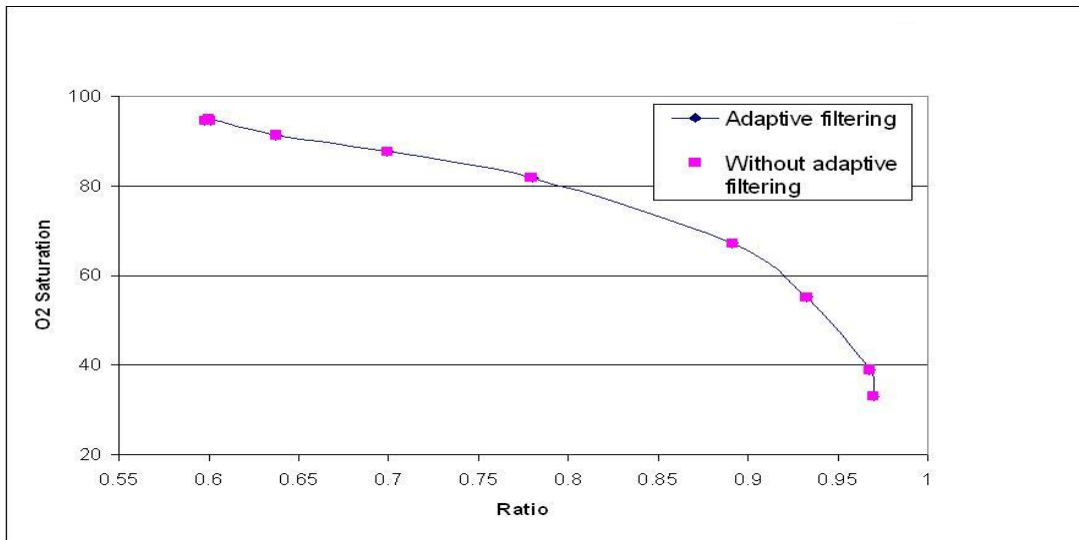


**Fig. 34.** Plot of oxygen saturation vs ratio in the *in vitro* experiment showing increasing oxygenation ratio with decreasing oxygen saturation

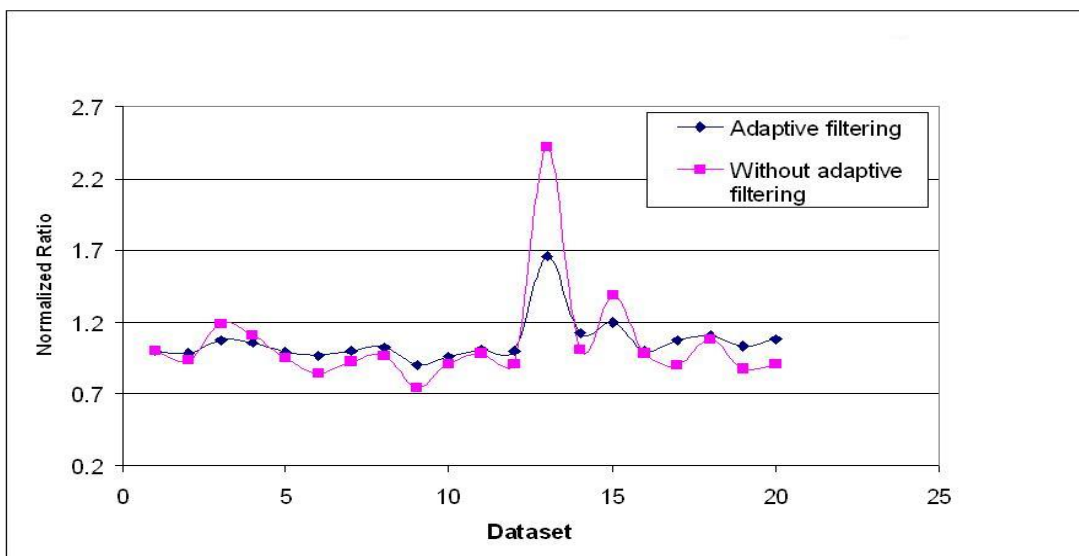


**Fig. 35.** Plot of oxygen saturation vs ratio in the *in vivo* experiment showing more stable oxygenation ratio from adaptive filtering

Statistically, when comparing the standard deviation from the mean of the data sets (Table 3), the adaptive filtering and autocorrelation algorithm yields an error of 0.088, which is roughly one half that of the autocorrelation alone (0.192). If data points 13-16 (previously explained to be erroneous due to no flow) are removed from the data set (Fig. 36) the error for the combined algorithm (0.056) still remains significantly lower than the autocorrelation algorithm (0.127).

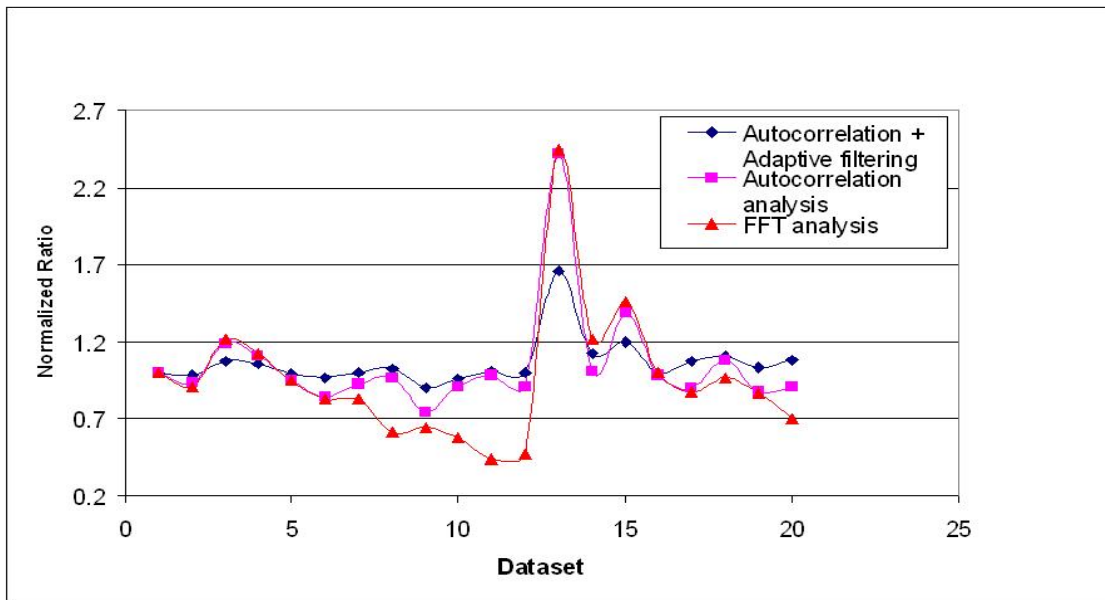


**Fig. 36.** Oxygenation ratio from different analysis techniques showing stable oxygenation ratio compared to traditional analysis techniques

**Table 3:** Summary of the standard error of different analysis techniques

Standard Error	FFT technique	Autocorrelation	Autocorrelation + Adaptive filtering
Entire data set	0.277752	0.192491	0.087645
Without low perfusion states	0.203736	0.127263	0.056408



## CHAPTER VI

### CONCLUSIONS AND FUTURE WORK

An autocorrelation based perfusion analysis algorithm has been developed to obtain the peak amplitude of both periodic and semi- periodic signals. It has been shown to work well for simulated, *in vitro*, and *in vivo* signals. The time domain technique that is currently being used to analyze pulse oximetry signals (weighted averaging) requires the knowledge of the repetition of the signal in order to obtain the amplitude. In the general case for biological signals with low signal-to-noise ratio, the repetition is obtained from a reference source, such as the heart rate using an electrocardiogram (ECG) or pressure sensor [9]. The APAA method was able to obtain the heart rate from the autocorrelation method without the need of external devices. Also, the APAA has proven to be more consistent than a standard Fourier transform due to its ability to handle heart rate variability (semi-periodicity).

The adaptive filtering technique has been used in the pulse oximetry data to separate the oxygenation and blood perfusion signal occurring simultaneously in the detector side by the introduction of a third source centered at the isosbestic point. The ultimate goal of this work is to separate oxygenation saturation and perfusion signals *in vivo* with fluctuating and/or low perfusion states characteristic of organ transplant complications. Using a simplified Monte Carlo model it was realized that the 810nm source functioned well to eliminate the perfusion artifact from the composite signal and allowed previously developed autocorrelation algorithms to work better. This was confirmed using real biological tissue and whole blood in an *in vitro* setup where effects

due to saturation and perfusion could be analyzed independently. Lastly, using a swine model, the ability of the new processing algorithm was analyzed with changing perfusion states. The algorithm showed a repeatable and constant measurement for both perfusion and oxygenation with the exception of no flow in which case the oxygenation signal was not well predicted because of the lack of a signal.

The LMS adaptive filter algorithm is favored in this project due to its simplicity and less computation time to separate the perfusion and oxygenation from biological signals. On the contrary, the LMS algorithm has a relatively slow rate of convergence, making it incapable of improving the signal to noise ratio in rapidly varying environment. Although computationally complex, a recursive least square (RLS) adaptive noise reduction technique with rapid convergence could be attempted in future analysis. Future work should also focus on miniaturization of the sensor for implantation and incorporating the processing algorithms into the sensor for real time processing that will allow for continuous monitoring of patient perfusion and oxygenation saturation.

## REFERENCES

- [1] Scientific Registry of transplant recipients, [www.ustransplant.org](http://www.ustransplant.org), accessed November, 2003.
- [2] L.C. Junqueira, J. Carneiro, and R.O. Kelley, *Basic Histology*, Standford, CT: Appleton and Lange, 1998.
- [3] B. Dixon, B.L. Ibey, M.N. Ericson, M.A. Wilson, and G.L. Cote, "Monte Carlo modeling of perfusion monitoring," in *Proc. from SPIE Photonics West Conference*, San Jose, California, 2003, pp. 42-48.
- [4] M.N. Ericson, B.L. Ibey, S.J. Lee, M.A. Wilson, and G.L. Cote, "In vivo application of a minimally invasive oximeter based perfusion sensor," in *Proc. of the Second Joint IEEE EMBS/BMES Conference*, Houston, Texas, 2002, pp. 1789-1790.
- [5] T.L. Rush, R.Sankar and J. Scharf, "Signal processing methods for pulse oximetry," *Computers in Biology and Medicine*, vol. 26, pp. 143-159, 1996.
- [6] S. Lee, B. L. Ibey, M.N. Ericson, M.A. Wilson, and G.L. Cote, "Wavelet and Fast Fourier transform analysis of oximeter-based perfusion data," Submitted to *IEEE Transactions on Biomedical Engineering*, 2003
- [7] H.Subramanian, B.L. Ibey, M.N. Ericson, M.A. Wilson, and G.L. Cote, "An autocorrelation based time domain analysis technique for monitoring perfusion and oxygenation in transplanted organs," Submitted to *IEEE Transactions on Biomedical Engineering*, 2003.
- [8] H.Subramanian, B.L. Ibey, M.N. Ericson, M.A. Wilson, and G.L. Cote, "Real time separation of perfusion and oxygenation signals for an implantable sensor using adaptive filtering," Submitted to *IEEE Transactions on Biomedical Engineering*, 2004.
- [9] J.G. Webster, *Design of Pulse Oximeters*, Philadelphia, PA: Institute of Physics Publishing, 1997.
- [10] L. Sherwood, *Human Physiology from Cells to Systems*, Florence, KY: Brooks/Cole, 2004.
- [11] Oxygen transport and the oxyhemoglobin disassociation cure, [www.asthma.about.com](http://www.asthma.about.com), accessed February, 2004.

- [12] D.W. Hill, *Methods of Measuring Oxygen Content of Blood Oxygen Measurements in Blood and Tissues and their Significance*, Boston, MA: Little Brown, 1966.
- [13] A.P. Adams and C.E.W Hahn, *Principles and Practice of Blood-gas Analysis*, New York: Churchill Livingstone, 1982.
- [14] A. Zwart, A. Buursma, B. Oeseburg and W.G. Zijlstra, "Determination of hemoglobin derivatives with the IL-282 CO-oximeter as compared with a manual spectrophotometric five wavelength method," *Clinical Chemistry*, vol. 27, pp.1903-1906, 1981.
- [15] C.M. Rigsby, P.M. Burns, B.B. Weltin, B. Chen and K.J.W. Taylor, "Doppler signal quantitation in renal allografts: comparison in normal and rejecting transplants with pathologic correlation," *Radiology*, vol. 162, pp. 39-42, 1987.
- [16] H. Kvernmo, A. Stefanovska, M. Braeie, K.A. Kirkeboen and K. Kvernebo, "Spectral analysis of the laser Doppler perfusion signal in human skin before and after exercise," *Microvascular Research*, vol. 56, pp. 173-182, 1998.
- [17] M. Nitzan, A. Babchenko, B. Khanokh, and D. Landau, "The variability of the photoplethysmographic signal – a potential method for the evaluation of the autonomic nervous system," *Physiologic Measurement*, vol. 19, pp. 93-102, 1998.
- [18] C. Dumas, J. Wahr, and K.K. Tremper, "Clinical evaluation of a prototype motion-artifact-resistant pulse oximeter in the recovery room," *Anesthesia and Analgesia*, vol. 83, pp. 269-272, 1996.
- [19] J.R. Squire, "Instrument for measuring quantity of blood and its degree of oxygenation in web of the hand," *Clinical Science*, vol. 4, pp. 331-339, 1940.
- [20] E.H. Wood, and J.E. Geraci, "Photoelectric determination of arterial saturation in man," *Journal of Lab Clinical Medicine*, vol. 34, pp. 387-401, 1949.
- [21] C.R. Stephen, H.M. Slater, A.L. Johnson, and P. Sekelj, "The oximeter – A technical aid for the anesthesiologist," *Anesthesiology*, vol. 12, pp. 541-555, 1951.
- [22] M.R. Flick, and A.J. Block, "In vivo continuous arterial oxygen saturation measurements by oximetry," *American Review of Respiratory Diseases*, vol. 113, pp. 113-126, 1976.
- [23] R. Peter, "In vivo near-infrared spectroscopy," *Annual Review of Biomedical Engineering*, vol. 2, pp. 715-754, 2000.

- [24] L.J. Bron, "A new instrument for the simultaneous measurement of total hemoglobin, % oxyhemoglobin, %carboxyhemoglobin, % methemoglobin, and oxygen content in whole blood," *IEEE Transaction on Biomedical Engineering*, vol. 27, pp. 132-138, 1980.
- [25] D.C. Buchanan, "Endotracheal tube with oxymetry means," U.S. Patent 5 005 573, 1991.
- [26] J.P. Payne and J.W. Severinghaus, *Pulse Oximetry*, New York: Springer, 1986.
- [27] P.H. Macdonald, and P.K. Dinda, "The use of pulse oximetry in determining intestinal blood flow," *Surgery*, vol. 76, pp. 451-458, 1993.
- [28] L.A. Lindsey, J.D.D. Watson and A.A. Quaba, "Pulse oximetry in postoperative monitoring of free muscle flaps," *British Journal of Plastic Surgery*, vol. 44, pp. 27-29, 1991.
- [29] C.L.L. Pope and D.V. Hankins, "Pulse oximetry: application in the labor and delivery unit of a tertiary care center," *Journal of Reproductive Medicine*, vol. 36, pp. 853-856, 1991.
- [30] C. Chung and H.M. McNamara, "Fetal pulse oximetry apparatus and method of use," US patent 5,228,440, 1993.
- [31] D.L. Reich, and A. Timcenko, "Predictors of pulse oximetry data failure," *Anesthesiology*, vol. 84, pp. 859-864, 1996.
- [32] A.R. Visram, R.D.M. Jones, M.G. Irwin, and J.B. Shone, "Use of two oximeters to investigate a method of movement artifact rejection using plethysmographic signals," *British Journal of Anaesthesiology*, vol. 72, pp. 388-392, 1994.
- [33] B.H. Yang and S.Rhee, "Development of the ring sensor for healthcare automation," *Robotics Autonomic System*, vol. 30, pp. 273-281, 2000.
- [34] R.J. Gush and T.A. King, "Discrimination of capillary and arterio-venular blood flow in skin by laser Doppler flowmetry," *Medical & Biological Engineering and Computing*, vol. 29, pp. 387-382, 1991.
- [35] A. Eke, and P. Herman, "Physiological time series: distinguishing fractal noises from motions," *European Journal of Physiology*, vol. 439, pp. 403-415, 2000.
- [36] C. Kasai and K. Namekawa, "Real time two dimensional blood flow imaging using an autocorrelation technique," *IEEE Transactions on Sonic and Ultrasonics*, vol. 32, pp. 458-464, 1985.

- [37] Y. Aizu and T. Asakura, "Compensation of eye movements in retinal speckle flowmetry using flexible correlation analysis based on the specific variance," *Journal of Biomedical Optics*, vol. 3, pp. 227-236, 1998.
- [38] L. Molegedey and H.G. Schuster, "Separation of a Mixture of Independent Signals Using Time Delayed Correlation," *Physical Review Letters*, vol. 72, pp. 3634-3637, 1994.
- [39] F.M. Coetzee and Z. Elghazzawi, "Noise resistant pulse oximetry using a synthetic reference signal," *IEEE Transactions on Biomedical Engineering*, vol.47, pp. 1018-1026, 2000.
- [40] M.K. Diab, K. Azerbayjany, and W.M. Weber, "Signal processing apparatus," U.S. Patent 5 490 505, Feb. 1996.
- [41] M.K. Diab, and K. Azerbayjany, "Signal processing apparatus and method," U.S. Patent 5 482 036, Jan. 1996.
- [42] I. Thaler, D. Shavit, and D. Adam, "Arrangement of time-sequenced adaptive filters for a complete fetal ECG morphology recording," in *Proc. of Computers in Cardiology*, Jerusalem, Israel, 1989, pp. 273-274.
- [43] Raya and L.G. Sison, "Adaptive noise canceling of motion artifacts in stress ECG signals using accelerometer," in *Proc. of the 2<sup>nd</sup> Joint EMBS/BMES Conference*, Houston, Texas, 2002, pp. 1756-1757.
- [44] A.R. Relente, L.G. Sison, "Characterization and adaptive filtering of motion artifacts in pulse oximetry using accelerometers," in *Proc. of the 2<sup>nd</sup> Joint EMBS/BMES Conference*, Houston, Texas, 2002, pp. 1769-1770.
- [45] International Union of Pure and Applied Chemistry, [www.iupac.org/goldbook/I03310.pdf](http://www.iupac.org/goldbook/I03310.pdf), accessed February, 2004.
- [46] B.L. Ibey, S.J. Lee, M.N. Ericson, M.A. Wilson, and G.L. Cote, "Modeling of a three-source perfusion and blood oxygenation sensor for transplant monitoring using Multi-Layer Monte Carlo code," in *Proc. from SPIE Photonics West Conference*, San Jose, California, 2003, pp. 62-69.
- [47] M. Hammer, E.Thamm and D.Schweizer, "A simple algorithm for *in vivo* ocular fundus oximetry compensating for non-haemoglobin absorption and scattering," *Physics in Medicine and Biology*, vol. 47, pp. 233-238, 2002.

- [48] R.P. Buinevicius, "A three wavelength pulse oximeter for carboxyhemoglobin determination," Masters thesis, Department of Electrical and Computer Engineering, University of Wisconsin-Madison (1987).
- [49] J.G. Proakis and D.G. Manolakis, *Digital Signal Processing – Principles, Algorithms and Applications*, Upper Saddle River, NJ: Prentice Hall Publications, 2003.
- [50] S.M. Kuo and D.R. Morgan, *Active Noise Control Systems – Algorithms and DSP Implementations*, New York: Wiley, 1996.
- [51] S.Haykin, *Adaptive Singal Processing*, Englewood Cliffs, NJ: Prentice-Hall, 1996.
- [52] M. Keijzer, S.L. Jacques, S.A. Prahl and A.J. Welch, "Light distributions in artery tissue: Monte Carlo simulations for finite-diameter laser beams," *Lasers Surgery and Medicine*, vol. 9, pp. 148-154, 1989.
- [53] I. Lux and L. Kobling, *Monte Carlo Particle Transport Methods: Neutron and Photon Calculations*, Boca Raton, FL: CRC Press, 1991.
- [54] L.H. Wang, S.L. Jacques and L. Zheng, "MCML – Monte Carlo modeling of light transport in multi-layered tissues," *Computer Methods and Programs in Biomedicine*, vol. 47, pp. 131-146, 1995.
- [55] L.G. Henyey and J.L. Greenstein, "Diffuse radiation in the galaxy," *Journal of Astrophysics*, vol. 93, pp. 70-83, 1941.
- [56] S.L. Jacques, C.A. Alter and S.A. Prahl, "Angular dependence of HeNe laser light scattering by human dermis," *Laser Life Science*, vol.1, pp. 309-333, 1987
- [57] J.S. Hendricks and T.E. Booth, "MCNP variance reduction overview," *Lecture Notes Physics*, vol. 240, pp. 83-92, 1985.
- [58] G. Yao and L.H. Wang, "Monte Carlo simulation of an optical coherence tomography signal in homogeneous turbid media," *Physics in Medicine and Biology*, vol. 44, pp. 2307-2320, 1999.
- [59] J.P Ritz and A.Roggan, "Optical properties of native and coagulated porcine liver tissue between 400-2400nm," *Lasers in Surgery and Medicine*, vol. 29, pp. 205-212, 2001.
- [60] A. Roggan, M. Friebel, and K. Dorschel, "Optical properties of circulating human blood in the wavelength range 400-2500nm," *Journal of Biomedical Optics*, vol.4, pp. 36-46, 1999.





## APPENDIX B

### MATLAB PROGRAM *apaa.m*

```

%apaa.m
clear all
w = load(uigetfile('*.txt'));
x = w(:,2);
har = x;
%constructing a bandpass filter
%-----
[b,a] = butter(4,[1.5 5]/150);
x_filt = filter(b,a,x);

%For detecting the frequency from FFT to verify the value obtained
%-----
x = x_filt(601:15000);
z = x-mean(x);
%-----

leng_samp = length(z);
sfreq_samp = 300;
n_samp = (leng_samp/2);

%autocorrelation of non periodic signal
%-----
[c_x,lags] = xcorr(z,n_samp,'coeff');
lags_z = lags(n_samp+200:2*n_samp+1);
c_z = c_x(n_samp+200:2*n_samp+1)+1;
%-----

%-----
init = 1;
count = 1;

%To find the distance between two peaks in autocorrelation
%-----
n_corr = length(c_z);
for k = 1:n_corr-1
    s(k+1) = (c_z(k+1)-c_z(init))^2;
    if s(k+1)<s(k)
        diff = c_z(k) - c_z(init);
        if diff < 0
            init = k;
            s(k+1) = (c_z(k+1)-c_z(init))^2;
        elseif diff > 0.01
            init = k;
            maxi(count) = lags_z(init);
            corr_max(count) = c_z(init);
            count = count+1;
            s(k+1) = (c_z(k+1)-c_z(init))^2;
        end
    end
end

```



## APPENDIX C

### MATLAB PROGRAM *Simultanalsel.m*

```

%Simultanalsel.m
clear all
w = load(uigetfile('*.txt'));
x = w(:,2);

%constructing a bandpass filter
%-----
[b,a] = butter(4,[1.5 5]/150);
x_filt = filter(b,a,x);

x_filt = x_filt(601:15000);

z_filt = x_filt-mean(x_filt);
leng_z = length(z_filt);
leng_samp = leng_z/12;
inc = 0;
    for h = 1:12
        z = z_filt((1:leng_samp)+inc);
        sfreq_samp = 300;
        n_samp = (leng_samp/2);

        figure(h+10);
        subplot(2,1,1);
        plot(x);
        xlabel('Time(sec)');
        ylabel('Amplitude');

%autocorrelation of non periodic signal
%-----
[c_x,lags] = xcorr(z,n_samp,'coeff');
lags_z = lags(n_samp+200:2*n_samp+1);
c_z = c_x(n_samp+200:2*n_samp+1)+1;
subplot(2,1,2);
plot(lags_z,c_z);
xlabel('Lags');
ylabel('Normalized amplitude');
%-----

%-----
init = 1;
count = 1;

%To find the distance between two peaks in autocorrelation
%-----
n_corr = length(c_z);
for k = 1:n_corr-1
    s(k+1) = (c_z(k+1)-c_z(init))^2;
    if s(k+1)<s(k)

```

```

diff = c_z(k) - c_z(init);
if diff < 0
    init = k;
    s(k+1) = (c_z(k+1)-c_z(init))^2;
elseif diff > 0.01
    init = k;
    maxi(count) = lags_z(init);
    corr_max(count) = c_z(init);
    count = count+1;
    s(k+1) = (c_z(k+1)-c_z(init))^2;
end
end
end

%-----
period = (maxi(2)-maxi(1))/sfreq_samp;

freq(h) = 1/abs(period);

size_window = period*sfreq_samp;

%Mamimum and minimum points from raw signal
%-----
index_x = 0;
count = 1;
while index_x < leng_samp-3*size_window

    t_window = (1:size_window)+index_x;
    max_x(count) = max(x(t_window));
    for index = t_window
        if x(index) == max_x(count)
            index_x = index;
            max_t(count) = index;
        end
    end
    t_window = (1:size_window)+index_x;
    min_x(count) = min(x(t_window));
    for index = t_window
        if x(index) == min_x(count)
            index_x = index;
            min_t(count) = index;
        end
    end

    mag_signal(count) = max_x(count)-min_x(count);

    figure(h+20);
    plot(x);
    plot([max_t(count),min_t(count)],[max_x(count),min_x(count)], 'bo');
    hold on;
    count = count+1;
end

mean_mag = mean(mag_signal);

```



## APPENDIX D

### MATLAB PROGRAM *LMSadaptive.m*

```

%LMSadaptive.m
clear all;
clf;

load a660.txt -ascii
load a810.txt -ascii
load a940.txt -ascii
load p660.txt -ascii
load p810.txt -ascii
load p940.txt -ascii
%Y = input('Enter the frequency you want the perfusion and oxygenation
signals to be at');
Y = 4;
Time = 1/Y;
Spacing = Time/6;
Duration = 50/Spacing;
%Red 660
%Oxygenation
g = 0;
n = 0;
for i = 1:12
    if i < 7
        absorb660(i) = a660(i);
    else
        j = (i-7)+(i-6);
        absorb660(i) = a660(i-j);
    end
end
for i = 1:Duration
    j = 12*g;
    absorb660a(i) = absorb660(i-j);
    n = n+1;
    if n == 12
        g = g+1;
        n=0;
    end
end
%Perfusion
g = 0;
n = 0;
for i = 1:12
    if i < 7
        perf660(i) = p660(i);
    else
        j = (i-7)+(i-6);
        perf660(i) = p660(i-j);
    end
end
end

```

```

for i = 1:Duration
    j = 12*g;
    perf660a(i) = perf660(i-j);
    n = n+1;
    if n == 12
        g = g+1;
        n=0;
    end
end
end
% Isobestic Point
%Oxygenation
g = 0;
n = 0;
for i = 1:12
    if i < 7
        absorb810(i) = a810(i);
    else
        j = (i-7)+(i-6);
        absorb810(i) = a810(i-j);
    end
end
end
for i = 1:Duration
    j = 12*g;
    absorb810a(i) = absorb810(i-j);
    n = n+1;
    if n == 12
        g = g+1;
        n=0;
    end
end
end
%Perfusion
g = 0;
n = 0;
for i = 1:12
    if i < 7
        perf810(i) = p810(i);
    else
        j = (i-7)+(i-6);
        perf810(i) = p810(i-j);
    end
end
end
for i = 1:Duration
    j = 12*g;
    perf810a(i) = perf810(i-j);
    n = n+1;
    if n == 12
        g = g+1;
        n=0;
    end
end
end
%Infrared 940
%Oxygenation
g = 0;
n = 0;

```

```

for i = 1:12
    if i < 7
        absorb940(i) = a940(i);
    else
        j = (i-7)+(i-6);
        absorb940(i) = a940(i-j);
    end
end
for i = 1:Duration
    j = 12*g;
    absorb940a(i) = absorb940(i-j);
    n = n+1;
    if n == 12
        g = g+1;
        n=0;
    end
end
%Perfusion
g = 0;
n = 0;
for i = 1:12
    if i < 7
        perf940(i) = p940(i);
    else
        j = (i-7)+(i-6);
        perf940(i) = p940(i-j);
    end
end
for i = 1:Duration
    j = 12*g;
    perf940a(i) = perf940(i-j);
    n = n+1;
    if n == 12
        g = g+1;
        n=0;
    end
end
save ab660.txt absorb660a -ascii
save ab810.txt absorb810a -ascii
save ab940.txt absorb940a -ascii
save pf660.txt perf660a -ascii
save pf810.txt perf810a -ascii
save pf940.txt perf940a -ascii
for i = 1:1200
    abs660a(i) = absorb660a(i)/absorb660a(1);
    abs810a(i) = absorb810a(i)/absorb810a(1);
    abs940a(i) = absorb940a(i)/absorb940a(1);
    pe660a(i) = perf660a(i)/perf660a(1);
    pe810a(i) = perf810a(i)/perf810a(1);
    pe940a(i) = perf940a(i)/perf940a(1);
end
j=0.5;
k=10;
compos660 = (j*abs660a)+(k*pe660a);

```



```

compos810 = (j*abs810a)+(k*pe810a);
compos940 = (j*abs940a)+(k*pe940a);
compos660 = compos660-mean(compos660);
compos810 = compos810-mean(compos810);
compos940 = compos940-mean(compos940);
compos660 = compos660/max(compos660);
compos940 = compos940/max(compos940);
compos810 = compos810/max(compos810);

modoxy660=j*(abs660a-mean(abs660a));
modoxy810=j*(abs810a-mean(abs810a));
modoxy940=j*(abs940a-mean(abs940a));
modpe660=k*(pe660a-mean(pe660a));
modpe810=k*(pe810a-mean(pe810a));
modpe940=k*(pe940a-mean(pe940a));

w1=compos660;
w2=compos810;
w3=compos940;

%*****
%Extracting perfusion signal of Red - using ANC LMS algorithm
reference = w2;      % 810 is the reference signal
primary = w1;       % 660 is the primary signal

samp_length = length(primary);
mu = 0.05;
N = 32;
window = samp_length/N;
w_lms = zeros(1,N);
output = zeros(1,N);
width = 0;
init = 0;
for iteration = 1:window
    primary_lms = primary ((1:N)+width);
    reference_lms = reference ((1:N)+width);
    w_lms(1) = init;
    for i=1:N-1;
        output(i) = reference_lms(i) - w_lms(i)*((primary_lms(i)));
        w_lms(i+1) = w_lms(i) + mu*primary_lms(i)*output(i);
    end
    init = w_lms(i+1);
    filt_coeff((1:N)+width) = w_lms;
    w1_prf((1:N)+width) = primary_lms.*w_lms;
    width = width + N;
end;

%Extracting perfusion signal of IR - using ANC LMS algorithm
reference = w2;      % 810 is the reference signal
primary = w3;       % 940 is the primary signal

samp_length = length(primary);
mu = 0.05;
N = 32;

```

```

window = samp_length/N;
w_lms = zeros(1,N);
output = zeros(1,N);
width = 0;
init = 0;
for iteration = 1:window
    primary_lms = primary ((1:N)+width);
    reference_lms = reference ((1:N)+width);
    w_lms(1) = init;
    for i=1:N-1;
        output(i) = reference_lms(i) - w_lms(i)*((primary_lms(i)));
        w_lms(i+1) = w_lms(i) + mu*primary_lms(i)*output(i);
    end
    init = w_lms(i+1);
    filt_coeff((1:N)+width) = w_lms;
    w3_prf((1:N)+width) = primary_lms.*w_lms;
    width = width + N;
end;
%Extracting perfusion signal of 810 - using ANC LMS algorithm
reference = w2;          % 810 is the reference signal
primary = w2;           % 810 is the primary signal

samp_length = length(primary);
mu = 0.05;
N = 32;
window = samp_length/N;
w_lms = zeros(1,N);
output = zeros(1,N);
width = 0;
init = 0;
for iteration = 1:window
    primary_lms = primary ((1:N)+width);
    reference_lms = reference ((1:N)+width);
    w_lms(1) = init;
    for i=1:N-1;
        output(i) = reference_lms(i) - w_lms(i)*((primary_lms(i)));
        w_lms(i+1) = w_lms(i) + mu*primary_lms(i)*output(i);
    end
    init = w_lms(i+1);
    filt_coeff((1:N)+width) = w_lms;
    w2_prf((1:N)+width) = primary_lms.*w_lms;
    width = width + N;
end;

w1_oxy = w1_prf+compos660;
w3_oxy = compos940-w3_prf;

```

```

%*****
%END OF PROGRAM FOR DESIGNING ADAPTIVE FILTER
%*****

```

## APPENDIX E

### MATLAB PROGRAM *Separatesignal.m*

```

%Separatesignal.m
%load data
%%%%%%%%%%%%%%%%%%%%%%%%%%%%%%%%%%%%%%%%%%%%%%%%%%%%%%%%%%%%%%%%%%%%%%%%
wave= [660 810 940];
pre = ['072903_1_SN201_Liver'];
v= ['Vrms'];
normal1=[];normal2=[];normal3=[];normal11=[];normal22=[];normal33=[];
normal_prf1=[];normal_prf2=[];normal_prf3=[];
t=1:1;
for i = 1:1
    temp=int2str(i);
    name1=[pre temp '_' int2str(wave(1)) '.txt'];
    name2=[pre temp '_' int2str(wave(2)) '.txt'];
    name3=[pre temp '_' int2str(wave(3)) '.txt'];
    name4=[pre temp '_' int2str(wave(1)) v '.txt'];
    name5=[pre temp '_' int2str(wave(2)) v '.txt'];
    name6=[pre temp '_' int2str(wave(3)) v '.txt'];

    w1=load(name1);
    w2=load(name2);
    w3=load(name3);
    wd1=load(name4);
    wd2=load(name5);
    wd3=load(name6);

    w1=w1(:,2);m1=mean(w1);
    w2=w2(:,2);m2=mean(w2);
    w3=w3(:,2);m3=mean(w3);
    wd1=wd1(:,2);
    wd2=wd2(:,2);
    wd3=wd3(:,2);
    mwd1=mean(wd1);
    mwd2=mean(wd2);
    mwd3=mean(wd3);
    mwd1=sqrt(2)*mean(wd1);
    mwd2=sqrt(2)*mean(wd2);
    mwd3=sqrt(2)*mean(wd3);

    fw1=fft(w1);
    fw2=fft(w2);
    fw3=fft(w3);

p1=abs(fw1(201))/7500;p2=abs(fw2(201))/7500;p3=abs(fw3(201))/7500;
    normal1 = [normal1 mwd1];
    normal2 = [normal2 mwd2];

```

```

normal3 = [normal3 mwd3];
normal11=[normal11 p1];
normal22=[normal22 p2];
normal33=[normal33 p3];

%*****
%Extracting perfusion signal of Red - using ANC LMS algorithm

reference = w2;      % 810 is the reference signal
primary = w1;       % 660 is the primary signal
mu = 0.05;
N = length(w1);
w = zeros(1,N);
output = zeros(1,N);
for i=1:N-1;
    output(i) = reference(i) - w(i)*((primary(i)));
    w(i+1) = w(i) + mu*primary(i)*output(i);
end
w1_prf = primary.*w';
%Extracting perfusion signal of IR - using ANC LMS algorithm
reference = w2;      % 810 is the reference signal
primary = w3;       % 940 is the primary signal
mu = 0.05;
N = length(w3);
w = zeros(1,N);
output = zeros(1,N);
for i=1:N-1;
    output(i) = reference(i) - w(i)*((primary(i)));
    w(i+1) = w(i) + mu*primary(i)*output(i);
end
w3_prf = primary.*w';
%Extracting perfusion signal of 810 - using ANC LMS algorithm
reference = w2;      % 810 is the reference signal
primary = w2;       % 810 is the primary signal
mu = 0.05;
N = length(w2);
w = zeros(1,N);
output = zeros(1,N);
for i=1:N-1;
    output(i) = reference(i) - w(i)*((primary(i)));
    w(i+1) = w(i) + mu*primary(i)*output(i);
end
w2_prf = primary.*w';

%*****
fw1_prf=fft(w1_prf);
fw2_prf=fft(w2_prf);
fw3_prf=fft(w3_prf);
p1_prf=abs(fw1_prf(201))/7500;
p2_prf=abs(fw2_prf(201))/7500;
p3_prf=abs(fw3_prf(201))/7500;

normal_prf1=[normal_prf1 p1_prf];
normal_prf2=[normal_prf2 p2_prf];

```



## VITA

Hariharan Subramanian was born in Madras, India on November 30, 1979 to Subramanian and Jayanthi. His high school education was done at S.R.M. Nightingale Higher Secondary School, Madras. After graduating from high school, he entered Hindustan College of Engineering, affiliated with the University of Madras in 1997. He majored in electronics and communication engineering and graduated with distinction in the year 2001. In the fall of 2001 he joined the Biomedical Sciences Division at Sri Ramachandra Medical University in Madras, and started working on a project funded by the Indo-French Center for the Promotion of Advanced Research (IFCPAR) to study the Inter-Relationship of Brain Activities using Optical sensors. In September 2002, he joined Texas A&M University and worked in the Optical Biosensing Laboratory under Dr. Gerard Cote'. He received Master of Science degree in biomedical engineering in December of 2004.

Mailing Address: 703 Gaytha Circle, #G, Bryan, TX-77801.

Permanent Address: No.5, F-2, Subramanian Street,  
West Mambalam, Chennai – 600 033,  
Tamil Nadu, India.

E-mail: hariharan\_79@hotmail.com